Online Estimation of Rolling Resistance and Air Drag for Heavy Duty Vehicles

Robin Andersson

Master of Science Thesis MMK 2012:41 MDA 431
KTH Industrial Engineering and Management
Machine Design
SE-100 44 STOCKHOLM

KTH Industrial Engineering and Management

Master of Science Thesis MMK 2012:41 MDA 431

Online Estimation of Rolling Resistance and Air Drag for Heavy Duty Vehicles

Robin Andersson

Approved	Examiner	Supervisor
2012-06-18	Jan Wikander	Bengt Eriksson
	Commissioner	Contact person
	Scania CV AB	Per Sahlholm

Abstract

The vehicle industry is moving towards more and more autonomous vehicles. In order to reduce fuel consumption and improve driver experience, driver support functions and vehicle control are becoming increasingly important. With information about the different parts of the driving resistance, driver support functions and vehicle control can be improved. The driving resistance can be divided into rolling resistance, air drag and change in potential energy due to road grade. Estimations of the road grade and the vehicle mass have been subject to many research publications and are used in numerous functions in heavy duty vehicles of today. With this information known, it is interesting to investigate the possibilities to estimate the rolling resistance and the air drag separately.

This thesis presents two methods based on Kalman filters for online estimation of the rolling resistance and the air drag. They both use information from sensors that are part of the standard equipment for heavy duty vehicles. A vehicle model is used together with measurements of the vehicle speed and information about the engine torque, the road grade and vehicle mass to generate the estimations. The designs of the estimators are described and the performance is evaluated through simulations and experiments with real vehicles.

The experiments have shown the difficulty in separation of the rolling resistance and air drag. It is shown that simultaneous estimations of the two is possible, but in practice a too large variation of speed is required to obtain accurate estimates with the investigated methods. It is also shown that when estimating one parameter at a time, accurate estimations can be generated. However, it is proven to be difficult to base these estimations on each other, to due large temperature dependency of the rolling resistance.

KTH Industriell teknik
och management

Examensarbete MMK 2012:41 MDA 431

Skattning av rullmotstånd och luftmotstånd för tunga fordon

Robin Andersson

Godkänt	Examinator	Handledare
2012-06-18	Jan Wikander	Bengt Eriksson
	Uppdragsgivare	Kontaktperson
	Scania CV AB	Per Sahlholm

Sammanfattning

Fordonsindustrin går mot alltmer autonoma fordon. Funktioner för fordonsreglering och förarstöd blir allt viktigare för att minska bränsleförbrukningen och förbättra förarupplevelsen. Med information om körmotståndets olika delar kan mer detaljerad information utnyttjas av funktioner som reglerar fordonen och deras prestanda kan därmed förbättras. Körmotståndet kan delas in i rullmotstånd, luftmotstånd samt förändring i potentiell energi orsakad av väglutning. Skattningar av väglutning och fordonets massa har förekommit i många forskningspublikationer och används idag i flertalet funktioner i tunga fordon. När information om dessa är känd kvarstår att undersöka möjligheten att skatta rullmotstånd och luftmotstånd var för sig.

I detta examensarbete presenteras två metoder baserade på Kalmanfiltrering för skattning av rullmotstånd och luftmotstånd. Båda metoderna använder information från sensorer som är vanligt förekommande på moderna tunga fordon. Skattningarna genereras genom att använda en fordonsmodell tillsammans med mätningar av fordonets hastighet samt information om motormoment, väglutning och fordonsvikt. En beskrivning av skattningsmetoderna ges och deras prestanda utvärderas genom simuleringar och experiment med riktiga fordon.

Experimenten visar att det är svårt att skilja rullmotstånd och luftmotstånd från varandra med de föreslagna metoderna. Det visas att simultana skattningar av både rull- och luftmotstånd är möjliga men att det i praktiken krävs en stor hastighetsvariation för att bra värden ska erhållas. Det visas också att skattning av en del av körmotståndet i taget genererar noggranna resultat. På grund av rullmotståndets kraftiga temperaturberoende visar det sig emellertid vara svårt att basera dessa skattningar på varandra.

Acknowledgements

This Master thesis has been carried out at the department of Vehicle Management Controls, REVM, at Scania CV AB in Södertälje, Sweden.

First I would like to thank my three supervisors at Scania. I thank Kim Mårtensson for his help, guidance and support during the project. Thanks to Per Sahlholm for his help and for the most valuable discussions we had over telephone. Thanks to Maria Södergren for her valuable help and guidance during the first half of the project.

Thanks also to Daniel Frylmark for giving me the opportunity to write this thesis and for making me feel at home at REVM. I would also like to thank the rest of the people at REVM and staff at other divisions at Scania for their valuable input and for making me feel welcome.

Finally I thank my supervisor at KTH, Bengt Eriksson for his inputs and for proofreading the report.

Robin Andersson
Stockholm, June 2012.

Nomenclature

Notations

Symbol	Description	Unit
α	Road grade	%
φ	Angle	rad
η	Gear efficiency	-
ρ_a	Mass density	kg/m^2
A_a	Area	m^2
c_d	Coefficient of air drag	-
c_r	Coefficient of rolling resistance	-
g	Gravity of Earth	m/s^2
i	Gear ratio	-
J	Moment of inertia	kgm^2
m	Mass	kg
r	Radius	m
T	Torque	Nm
v	Speed	m/s

Abbreviations

CAN	Controller Area Network
EKF	Extended Kalman filter
KF	Kalman filter
LSE	Least squares estimation
GPS	Global positioning system
RMSE	Root mean square error
WGN	White Gaussian noise

Contents

1 Introduction

The first section in this chapter describes the background to the project. The purpose of the project, the delimitations made and the method used are described in the subsequent sections. The last two sections gives a summary of results from the project and details the report outline.

1.1 Background

Information about the driving resistance that a vehicle experiences during driving is used in many functions in today's heavy duty vehicles in order to reduce fuel consumption and improve driver experience. The force from the total driving resistance can be divided into different parts with different origins:

- the force from the rolling resistance,
- the force from the air drag and
- the force from an increased potential energy due to positive road grade.

By performing online estimations of the different parts of the driving resistance, the fuel efficiency and driver experience can be improved by providing more detailed information to functions that are controlling the vehicle.

One common function is to adapt the speed of the vehicle based on information about upcoming road topography. The concept is illustrated in figure 1.1.

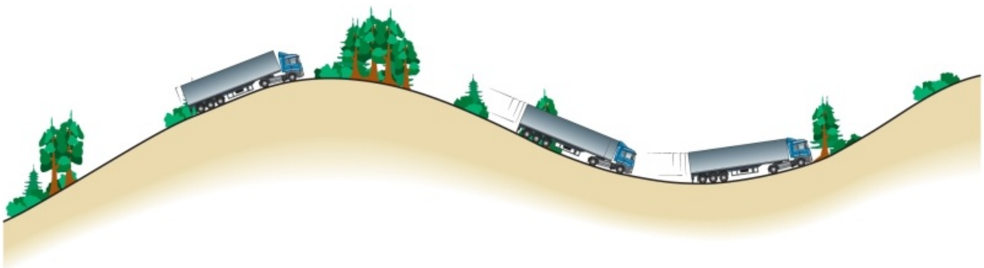

Figure 1.1: Illustration of a vehicle climbing and descending on a road. By adjusting the speed prior to uphill and downhill segments fuel savings can be made. Image courtesy of Scania CV AB.

When the vehicle is reaching the top of a hill and facing a downhill road segment, it is often advantageous to decrease the speed and utilize the gravity to obtain an acceleration. When driving on flat road and approaching an uphill road segment, the overall fuel economy can be improved by increasing the speed before the hill is reached. If the rolling resistance and air drag are known, more accurate predictions about the required engine torque at difference speeds can be made and the speed control can be further improved.

Other examples of functions that depend on predictions about future states are gearbox control for automatic gearboxes, control of auxiliary systems and control of hybrid vehicles.

There exists a large variety of different vehicle configurations, some of which are shown in figure 1.2. Due to differences in vehicle size, body shape and number of wheel axles a difference in rolling resistance and air drag between the vehicles could be expected. However, many functions are based on the assumption that the rolling resistance and air drag are the same regardless of vehicle configuration.

Therefore, online estimations of the different parts of the driving resistance can provide important information to functions that are controlling the vehicle.

Figure 1.2: Three different but commonly used vehicle configurations: a long-haulage timber truck and trailer, a streamlined tractor-semitrailer combination and a smaller distribution truck. Images courtesy of Scania CV AB.

1.2 Purpose

The purpose of the thesis is to suggest methods for real time estimation of rolling resistance and air drag on heavy duty vehicles.

1.3 Delimitations

The following delimitations and assumptions has been made for this thesis.

- Firstly, only longitudinal dynamics are considered. Sharp turns that introduces lateral forces which may increase the total driving resistance are not studied in the thesis.

- Secondly, it is assumed that the vehicle mass and the road grade are known. Estimations of both these parameters are made in the vehicles used in this thesis, and they are therefore considered to be known.
- Thirdly, no extensive tire modeling is made. Only existing tire models are studied in this thesis.
- Fourthly, since the suggested methods should be able to implement on standard modern heavy duty vehicles, they should only use information from sensors that are commonplace on such vehicles.

1.4 Method

The method used during the thesis starts with a background study including the definition of the frame-of-reference. The background study focus on gaining knowledge on vehicle dynamics and on the driving resistances that acts on a heavy duty vehicle during driving. Further, investigations of general methods for parameter estimation is an important part of the study.

After the background study, a number of methods to estimate the different parts of the driving resistance are developed. Two experiments are conducted where the first one takes place directly after the methods are formulated. The result from the first experiment is used to evaluate the suggested methods and the experiment itself. The focus of this experiment is on developing a good method for measuring the signals of interest.

Based on the results from the first experiment, the most promising methods are selected for further development and thereafter is the second experiment conducted. This experiment is focused on data acquisition from different vehicle configurations and driving scenarios. The planning and conducting of the second experiment takes advantage of experiences from the first experiment and thereby are improved results expected. With the use of the results from the second experiment, the selected methods are further developed.

This enables for an iterative work flow beneficial to the project in order to select, prioritize and develop the methods for solving the task.

1.5 Summary of Results

In this work it is shown that using an extended Kalman filter together with the derived nonlinear vehicle model for estimations of rolling resistance and air drag is possible. However, to obtain convergence of the estimations, a variation of speed larger than that found during ordinary driving scenarios is required. It is also shown that a standard Kalman filter when used together with the derived linearized vehicle model is able to generate accurate results when estimating only of the rolling resistance or the air drag. Basing estimates on each other is proven to be difficult due to a large temperature dependency of the rolling resistance.

1.6 Report Outline

Chapter 2 defines the frame-of-reference that has been used in this thesis and gives a general description of the studied system, details different models for rolling resistance and air drag, as well as introduces the concept of state reconstruction through observers and Kalman filters. A vehicle model is derived and simulated in Chapter 3. Chapter 4 details the design of the suggested estimations methods and describes the steps taken to tune the filters to generate accurate estimates. A description of the experiments used to develop and evaluate the methods is given in Chapter 5. The conclusions drawn from the experiments and a description of areas for future work is presented in Chapter 6.

2 Frame of Reference

This chapter provides an overview over the heavy duty vehicles (HDVs) used in this thesis, describes models for the rolling resistance and the air drag and introduces the concept of estimation through state observers.

2.1 System Description

The vehicles studied in this work are equipped with many different sensors that are commonly used with modern HDVs. The estimation methods presented in this thesis uses information from some of these sensors. The vehicles contain several control units which are connected via a data bus and forms a distributed system. An overview of some of these control units is given in figure 2.1.

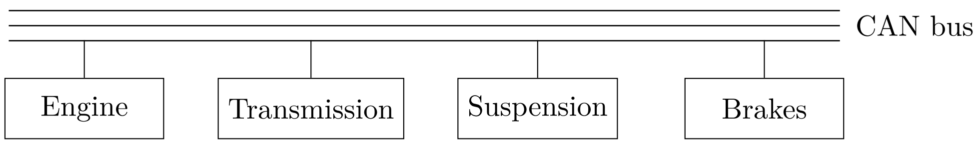

Figure 2.1: Schematic figure over a part of the distributed control system found in the HDVs.

The signals from the control units are broadcast on the data bus which in this case uses the Controller Are Network (CAN) protocol, a communication protocol commonly used in the vehicle industry. A description of CAN is found in the ISO standard (ISO 11898-1:2003, 2003).

For the estimators presented in this thesis, the interesting units are the engine control unit, the transmission control unit, the air suspension and the brake system. These are all connected to the CAN bus and broadcast signals from sensors and from estimations. The engine control unit broadcast the engine speed and engine torque. The transmission control unit broadcast the current gear and whether a gear shift occurs or not. From sensors in the air suspension are vehicle mass estimations performed. The brake system gives information about if any of the brakes are applied. The vehicle speed is obtained from sensors on the front axle.

2.2 Modelling

This section gives a description of the different models for the rolling resistance studied in this thesis and describes the equation for the force from the air drag.

2.2.1 Tire Modelling

Several tire models are presented in the literature. Common for most models however, is that the force from the rolling resistance of the tires is modelled as the normal force on the tires from the ground multiplied with the rolling resistance coefficient c_r. The equation is given in (Kiencke and Nielsen, 2003) as

$$F_{roll} = mgc_r \cos(\alpha) \approx mgc_r \tag{2.1}$$

where c_r is the rolling resistance coefficient, m is the vehicle mass, g is the gravity of earth and α is the road grade in percent. Expressing α in percent is common, not only in scientific publications but also on road signs. According to (Sahlholm, 2011), the relationship between road grade in percent and in radians (α_{rad}) is given by $\alpha_{rad} = \tan(\alpha/100)$. Road grades above 15 % are rare, and for normal roads is the road grade generally not above 6 %. For those grades, the small angle approximation in equation (2.1) is valid, and the difference between α and α_{rad} is negligible.

A nominal constant value of the coefficient for trucks as presented in (Sandberg, 2001) and (Sahlholm, 2011) is $c_r = 0.007$.

More sophisticated models of c_r include a speed dependence. In (Kiencke and Nielsen, 2003), a linear speed term is included,

$$c_r = c_{r,1} + c_{r,2}v \tag{2.2}$$

where v is the vehicle speed.

In (Wong, 2001) the rolling resistance coefficient instead includes a squared speed term dependence, given as

$$c_r = 0.006 + 0.23 \cdot 10^{-6}v^2 \tag{2.3}$$

As presented in (Sandberg, 2001), the tire manufacturer Michelin proposes a model of c_r that includes both a linear and a squared speed dependence, given by

$$c_r = c_{r,iso} + a\left(v^2 - v_{iso}^2\right) + b\left(v - v_{iso}\right) \tag{2.4}$$

where $c_{r,iso}$, a and b are tire dependent constants and $v_{iso} = 80$ [km/h].

Further in (Sandberg, 2001) a tire model is derived that includes both a velocity dependence as well as a temperature dependence, i.e.,

$$c_r = f\left(v, T\right) \tag{2.5}$$

The temperature dependence of the rolling resistance is also discussed in (Wong, 2001). It is shown that c_r decreases with an increasing tire temperature. It is stated that $c_r = 0.020$ when the tire temperature is 0°C, and approaches $c_r = 0.007$ as the temperature increases towards 80°C. However, the actual value of c_r also depends on the type of tire, the tire thread and how worn the tire is, as well as on the road surface.

In (Sandberg, 2001) it is also stated that the number of wheel axles does not influence c_r. Both the rolling resistance of the tires and the bearing losses from the bearings the wheels are mounted on are proportional to the mass. Therefore, it is stated that only the vehicle mass affects the total force from the rolling resistance, and not the number of wheel axles.

It can be concluded that several different types of tire models exist with considerably different behavior. The choice of model is discussed in section 3.2.2.

2.2.2 Air Drag Modelling

The force from the air drag is according to (Hucho et al., 1998) given by the equation

$$F_{airdrag} = \frac{1}{2}\rho_a c_d A_a v_{res}^2 \tag{2.6}$$

where ρ_a is the air mass density, c_d the air drag coefficient and A_a is the effective area of the vehicle. It is from this equation that c_d is defined and it is hence not an approximation of the force from the air drag. It is not specific for vehicles and is used to determine the force on any object moving through a fluid regardless of shape.

The vehicle velocity relative to the road is denoted by v, while the velocity of an occasional wind is denoted v_{wind}. When calculating the air drag, the resulting velocity, v_{res}, of the flow approaching the vehicle is of interest and is in (Hucho et al., 1998) given as the vector sum of the two velocities

$$v_{res} = \sqrt{v^2 + v_{wind}^2 + 2v \cdot v_{wind}\cos(\beta)} \tag{2.7}$$

$$\cos(\beta) = \frac{v_{res}^2 - v^2 - v_{wind}^2}{2v_{res} \cdot v} \tag{2.8}$$

Here, β is the angle between the vehicle velocity and the wind velocity.

The wind speed is generally difficult to measure on road since wind speed and direction sensors, commonly referred to as anemometers, are not easily mounted on a truck. Due to turbulence from the vehicle, see for example (Hucho et al., 1998), the anemometer would have to be placed either in front of, or high above the vehicle. In (Walston et al., 1976) an experiment is described where the anemometer is placed about 3 meters in front of the vehicle.

The air drag coefficient depends on the size and shape of the vehicle. In (Hucho et al., 1998) some nominal values of c_d for different types of vehicles are presented. For a tractor with a semi-trailer the values are between 0.48 to 0.75. For a truck and trailer the vales are a bit higher, 0.55 to 0.85.

When the vehicle travels in a windless environment, the effective vehicle area simply becomes the frontal area of the vehicle. When experiencing a crosswind on the other hand, the effective area becomes the vehicles projected area in the direction of the resulting air flow. The effect is the same when the vehicle is turning and a non-zero yaw angle is experienced.

The effect on the air drag coefficient from different yaw angles is presented in (Hucho et al., 1998). The values are normalized to the air drag coefficient at zero yaw angle. For a tractor with a semi-trailer, the normalized values of c_d for yaw angles of 10, 20 and 30 degrees are 1.25, 1.5 and 1.6 respectively. For a truck with a trailer the values are higher with a normalized value of 1.4 already at 10 degrees yaw angle. It is also stated that yaw angles over 10 degrees are rare when driving at higher speeds.

The value of c_d can be determined from wind tunnel tests. By studying typical wind conditions on roads and the size proportions compared to the speed of the vehicle, a statistically wind-averaged value of c_d can be determined. This is done by sweeping the vehicle with air flow between the relevant angles. The value of c_d is then calculated from equation 2.6 by measuring the force $F_{airdrag}$. A nominal statistically wind-averaged value of c_d for a typical tractor-semitrailer combination is reported by Scania to be $c_d = 0.6$. This value is based on the reference area $A_a = 10.4\text{m}^2$.

2.3 Earlier Related Work on Estimation of Vehicle Parameters

This section describes the coast down test, a method for offline estimations of the rolling resistance and air drag that is commonly used in the industry. A description of methods for online estimation of road grade and vehicle mass is also presented. These are important parameters that in this work are considered to be known. Further, the studied methods can be used for estimation of other vehicle parameters as well.

2.3.1 Coast Down Test

One common method to perform offline estimation of rolling resistance and air drag is the coast-down tests, described in (White and Korst, 1972). The general principle is to let the vehicles freely coast down from an initial speed, typically around 70-80 [km/h] to a speed of around 20 [km/h]. By measuring the distance covered, the instantaneous speed and the elapsed time, estimations of the parameters can be generated. If the road grade is unknown, the test should be performed on a flat road. In order to reduce influence from an occasional wind, the tests are usually performed several times in two opposite directions on the test surface. Another solution is presented in (Walston et al., 1976), where a coast down test procedure with an anemometer is presented. By using the anemometer to measure the wind speed and direction, the test can be performed even in windy conditions.

Based on the measured data and a model of the vehicle, a least squares estimation of the parameters can be performed. If care is taken to the experiment, this method has been showed to generate accurate results.

The coast down test is as mentioned a method for offline estimation which is not the purpose for this project. However, the method can be used to generate accurate estimations of the rolling resistance and the air drag that can be compared to online estimates generated with other methods. In section 4.4.2 a coast down test is described where the results are used to tune an online estimator.

2.3.2 Road Grade and Vehicle Mass

Estimation of road grade and vehicle mass have been subject to many articles and research papers. In (Sahlholm, 2011) methods for road grade estimation are presented. Two methods uses the Kalman filter and Extended Kalman filter, both commonly used for parameter estimation. These are described in detail in section 2.4.1. A Global Positioning System (GPS) is used to obtain altitude measurements which are incorporated in the estimators in order to generate accurate results. More information about GPS is given in (Misra and Enge, 2006). In (Vahidi et al., 2005) a recursive least squares estimation of both road grade and vehicle mass is presented. The recursive least squares estimation algorithm is given in (Kailath et al., 2000).

A method for measuring the road grade and estimating the vehicle mass as well as rolling resistance and air drag through a recursive least squares estimation is given in (Bae and Gerdes, 2003). Measurements of the road grade are obtained from a GPS. Although the suggested method showed good results for the road grade and vehicle mass, it is concluded that the estimations of neither the coefficient of rolling resistance or air drag converged.

In the vehicles used in this thesis, both vehicle mass and road grade estimations are performed online and are therefore considered to be known. Additionally, information about the road grade from map data is available from a commercial provider and broadcast on the vehicles CAN-network.

Although the estimations presented in the above works are made on different parameters than the ones considered in this thesis, the concept is still the same. A vehicle model is derived and a Kalman filter (recursive least squares is a special case of the Kalman filter) is used for the estimation. Studying the above works therefore gives useful knowledge that is applied in this project.

2.4 State Reconstruction

A common method for parameter estimation is to use an estimator (or observer). An estimator can be used to reconstruct the states of a system that cannot be measured (Glad and Ljung, 2000). Estimations of the systems internal states can be made based on knowledge of the systems input and output signals. The concept behind estimators is shown in figure 2.2. The systems in-

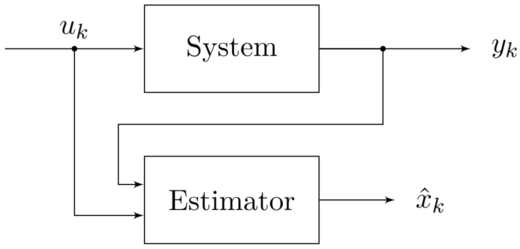

Figure 2.2: Block diagram over a system and estimator.

put and output signals are denoted u_k and y_k, respectively. Here, k is used to indicate discrete time. The system can be governed by a nonlinear expression

$$x_k = f\left(x_{k-1}, u_k, \omega_{k-1}\right) \tag{2.9}$$
$$y_k = h\left(x_k, e_k\right) \tag{2.10}$$

or a linear expression on state space form

$$x_k = Fx_{k-1} + Gu_k + \omega_{k-1} \tag{2.11}$$
$$y_k = Hx_k + e_k \tag{2.12}$$

where the column vector x_k contains the states of the system. The process noise ω_k has covariance $Q_k = E[\omega_k^2]$ and the measurement noise e_k has covariance $R_k = E[e_k^2]$, where E is the expected value.

In this work, it is assumed that the noise ω and e are white Gaussian noise (WGN). A definition of white noise is given in (Glad and Ljung, 2000). The interpretation is that white noise has a constant frequency spectrum and that the noise cannot be predicted, i.e., past noise contains no information on future noise. With white Gaussian noise it is indicated that the mean of the noise is zero and that it is normally distributed.

By using a model of the system and with knowledge of the input signal to the system, the estimator can simulate the states of the system, denoted $\hat{x}_k$. Since the output of the system is measured, it can be compared to the simulated output ($h(\hat{x}_k)$ or $H\hat{x}_k$) and the difference is used to correct the simulations. This yields the nonlinear estimator

$$\hat{x}_k = f\left(\hat{x}_{k-1}, u_k\right) + K\left(y_k - h(\hat{x}_{k-1})\right) \tag{2.13}$$

where K is the gain of the estimator. For a linear system the estimator becomes

$$\hat{x}_k = F\hat{x}_{k-1} + Gu_k + K\left(y_k - H\hat{x}_{k-1}\right) \tag{2.14}$$

Since the actual noise in each time step is unknown, the estimators are approximated without ω_k and e_k.

In (Glad and Ljung, 2006), it is shown that the estimator gain K affects both the dynamics of the error in the estimates as well as the sensitivity to measurement noise. This is easiest illustrated by studying the linear system. The error of the estimates is formed by $x_k^e = x_k - \hat{x}_k$. Inserting equations (2.11) and (2.14) it can be shown that the differential equation governing the error dynamics is given by

$$\hat{x}_k^e = \left(F - KH\right)\hat{x}_{k-1}^e + \omega_{k-1} - Ke_k \tag{2.15}$$

See (Glad and Ljung, 2006) for more details. From the expression it can be seen that if $(F - KH)$ is stable the estimation error will be reduced and the estimated states will converge towards the true values. If K is chosen so that the eigenvalues of $(F - KH)$ are far into the stability region the estimation error will quickly be reduced.

For a discrete time system, the stability region is defined as inside the unit circle, and a system is stable when its eigenvalues are inside or on the boundary of the stability region, (Glad and Ljung, 2000).

However, the size of K also affects the influence from the measurement noise e_k. There is hence a trade of between fast dynamics and noise sensitivity.

Several methods can be used to determine K. In the literature, for example (Glad and Ljung, 2000), it is stated that if the process and measurement noises are WGN, the corresponding covariance matrices are physically correct and the system is linear, then the optimal choice of K is given by the *Kalman filter*. Kalman filters are commonly used for various purposes and represent a state of the art method for tasks such as filtering noisy measurements, sensor fusion and, as in this case, parameter estimation. The next section gives a detailed description of the Kalman filter.

2.4.1 Kalman Filter

The Kalman filter (KF) is linear and the process model used with the KF therefore has to be either linear in its nature or a linearized representation of a nonlinear system. A commonly used method to deal with nonlinear systems is to perform linearizations at each time step. This results in the Extended Kalman filter (EKF). The discrete KF and EKF algorithms are given in (Kailath et al., 2000), and can be divided into two groups: the time update equations and the measurement update equations.

The notation $x_{k|k-1}$ is used to indicate the state x at time k given the information up until time $k-1$. The time update equations predicts the estimated states ($\hat{x}_{k|k-1}$) and estimated error covariance ($P_{k|k-1}$) for the next time step, and is for the KF given by

$$\hat{x}_{k|k-1} = F\hat{x}_{k-1|k-1} + Gu_k \tag{2.16}$$

$$P_{k|k-1} = FP_{k-1|k-1}F^T + Q_k \tag{2.17}$$

The EKF linearizes the system at each time step, but uses the nonlinear representation of the process model in the time update equation for the estimated states. The time update equations for the EKF therefore becomes

$$\hat{x}_{k|k-1} = f\left(\hat{x}_{k-1|k-1}, u_k\right) \tag{2.18}$$

$$P_{k|k-1} = F_k P_{k-1|k-1} F_k^T + Q_k \tag{2.19}$$

where $F_k = \frac{\partial f}{\partial x}(\hat{x}_{k-1|k-1}, u_k)$. This linearization follows the procedure described in section 4.1.1.

The measurement update equations are used to correct the estimated states and error covariance predicted in the time update equations by comparing the estimated states with the measurements. The equations are given by

$$K_k = P_{k|k-1}H_k^T\left(H_k P_k H_k^T + R_k\right)^{-1} \tag{2.20}$$

$$\hat{x}_{k|k} = \hat{x}_{k|k-1} + K_k\left(y_k - H_k\hat{x}_{x|x-1}\right) \tag{2.21}$$

$$P_{k|k} = \left(I - K_k H_k\right) P_{k|k-1} \tag{2.22}$$

where $H_k = \frac{\partial h}{\partial x}(\hat{x}_{k-1|k-1})$ for the EKF and $H_k = H$ for the KF, see equations (2.10) and (2.12).

The time update and measurement update equations are repeated recursively, and is given an initial value of $\hat{x}_k$ and P_k, denoted $\hat{x}_k^0$ and P_k^0.

Generally, a large initial value of P_k causes the filter react fast to large estimations errors in the beginning of the filtering. The gain K is calculated by the filters to minimize P_k. However, if the true value of the estimated state for some reason changes during estimation, a low value of P_k might cause the estimator to react slow to the change. The filter will eventually converge but might do so in a too long time frame.

If the earlier stated requirements on optimality for the filter are fulfilled, then $P_k = [x_k^e(x_k^e)^T]$. The magnitude of the diagonal elements in P_k is interpreted as the actual variance of the estimated states. However, as soon as the the noise becomes colored or Q_k and R_k deviates from the true values this interpretation fails. Therefore, in practical cases, it is often difficult to draw conclusions of the actual magnitude of P_k.

In (Höckerdal, 2011), it is stated that P_k for an unobservable mode increases linearly towards some value. This value might however be higher than what is possible to reach during estimations in practice. Studying P_k is therefore an important part of the analysis. The observability concept is given in section 2.4.2.

In most practical cases it is difficult to determine the process noise. Therefore the physically true Q_k and R_k are unknown and becomes tuning parameters for the filter. A large value of Q_k will cause the filter to believe less in the model, while a large R_k causes the filter react slower to the measurements. Section 4.4 describes the tuning steps for the filters used in this thesis.

2.4.2 Observability

Observability or detectability of the system to be estimated are important properties to ensure correct estimations from the observer. The observability criterion states that if a system is observable, the current states of the system can be reconstructed from measurements, see for example (Kailath et al., 2000). In the same place, several methods to determine observability are presented.

Observability of a Linear System

For a linear system in continuous time on state space form with n number of states

$$\dot{x}(t) = Ax(t) + Bu(t) \tag{2.23}$$

$$y(t) = Cx(t) \tag{2.24}$$

the observability of the system can be determined by calculating the rank of the $n \times n$ observability matrix $\mathcal{O}$. One common expression for this matrix given in (Kailath et al., 2000) as

$$\mathcal{O} = \begin{pmatrix} C \\ CA \\ \vdots \\ CA^n \end{pmatrix} \tag{2.25}$$

If this matrix has full column rank, i.e., if

$$rank\,(\mathcal{O}) = n \tag{2.26}$$

then the system is observable and can be used for parameter estimation.

Several other methods for calculating the observability matrix are given in (Kailath et al., 2000). In (Paige, 1981) numerical properties of these methods are discussed and it is stated that the matrix (2.25) is not the most numerically stable. However, since the number of states used in this work is low (two to three states), the method has shown to generate accurate results for the systems studied when compared to more numerically stable methods.

Observability of a Nonlinear System

For a nonlinear system, the observability matrix can be calculated, according to (Höckerdal, 2011), as the Jacobian of the matrix spanned by the Lie derivative L along the vector field f, i.e.,

$$\mathcal{O} = \begin{pmatrix} dh \\ dL_f h \\ \vdots \\ dL_f^{n-1} h \end{pmatrix} \tag{2.27}$$

A definition of the Lie derivative is given in (Glad and Ljung, 2000).

If the matrix $\mathcal{O}$ has full column rank the system is observable. The criterion hence is the same as for linear systems, i.e., if

$$rank\,(\mathcal{O}) = n \tag{2.28}$$

then the system is observable.

As described in section 2.4.1, the EKF linearizes the nonlinear system at each time step. According to (Glad and Ljung, 2000), a necessary condition when using an EKF for estimation is that the linearized system, i.e., the pair F_k and H_k, is detectable. The detectability criterion is given in (Kailath et al., 2000). There it is stated that if all of the unobservable modes of the system are stable, then the system is detectable.

The method to determine observability for the linear system used in the previous section, 2.4.2, can hence also be used to determine detectability.

Condition Number of the Observability Matrix

Even for an observable system, it can be more or less easy for the estimator to actually observe the states due to numerical properties, (Gustavsson, 2000). The condition number κ of the observability matrix can be interpreted as how difficult it is to observe the system states. One way to determine the condition number is presented in (Paige, 1981) as

$$\kappa(\mathcal{O}) = \frac{\sigma_{max}}{\sigma_{min}} \tag{2.29}$$

where σ_{max} and σ_{min} are the largest and smallest singular values of the observability matrix. The definition of singular values is given in (Glad and Ljung, 2000) as $\sigma = \sqrt{\lambda_i}$, where λ are the eigenvalues of the matrix A^*A, given a matrix A. For an ill-conditioned matrix it can be difficult to observe the states, even though the system is observable.

2.4.3 Discretization

Since the estimators are to be implemented on a digital system, derived continuous time models has to be discretized. For a linear system on state space form, a method for discretization is given in (Glad and Ljung, 2000) as

$$F = e^{AT_s}, \quad G = \int_0^{T_s} e^{At} B \; dt, \quad H = C \tag{2.30}$$

where T_s is the sampling time and A, B, and C are defined in equations (2.23) and (2.24). The matrix F is called the state transition matrix, G is the discrete control matrix and H is the measurement matrix. Further in (Glad and Ljung, 2000) it is stated that the discretization can be approximated with

$$F = I + AT_s, \quad G = BT_s \tag{2.31}$$

There are several methods to discretize a nonlinear system. In this work the Euler forward method is used, see for example (Glad and Ljung, 2006), given by

$$\dot{x}\,(kT_s) \approx \frac{1}{T_s}\,(x_{k+1} - x_k) \tag{2.32}$$

Although not stated as the most stable discretization method, it is explicit and therefore used in this work.

In (Kailath et al., 2000) it is stated that the observability of a system, described in section 2.4.2, is not lost during discretization as long as the sampling time is small enough.

2.4.4 Performance Measures

In order to determine the accuracy of the estimations, the root mean squared error (RMSE) is calculated, see for example (Gustavsson, 2000). It is given by

$$\text{RMSE} = \sqrt{\frac{1}{N}\sum_{i=1}^{N}(\hat{x} - x)^2} \tag{2.33}$$

where N is the number of data points, $\hat{x}$ the estimated state and x the true state. This method can thus only be used when the true value of the state is known.

3 Vehicle Model

This chapter derives the vehicle model which used in the estimations. The first section derives the equations for the vehicle driveline while the second section describes the external forces that acts on a vehicle during driving. The third section presents the complete vehicle model and a simulation of the model is presented in the last section.

3.1 Driveline Model

The vehicle driveline model used in this thesis is based on the model presented in (Kiencke and Nielsen, 2003). The equations describing the gear box gear ratios, efficiencies and the transmission and final drive are from (Sahlholm, 2011), and hence the final vehicle model presented here becomes identical to the model in (Sahlholm, 2011). Figure 3.1 shows the engine and driveline for a rear wheel driven vehicle. The notations used in the following expressions for the different parts of the driveline are defined in figure 3.2, which is based on the figures in (Kiencke and Nielsen, 2003) and (Sahlholm, 2011).

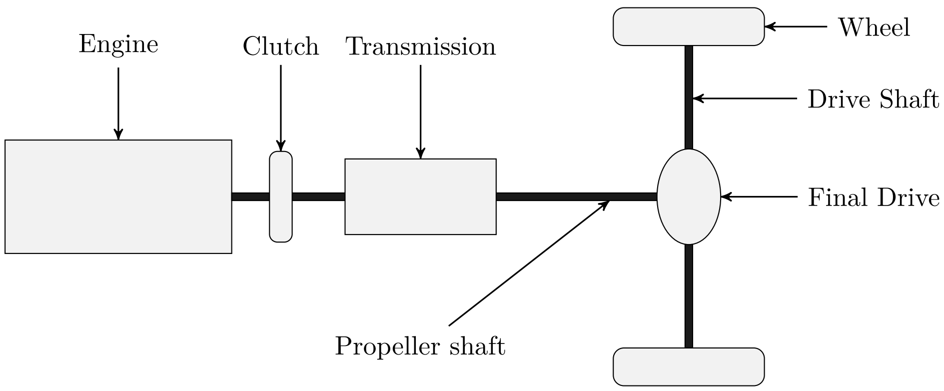

Figure 3.1: Schematic figure over the vehicle driveline. This figure is based on the figure in (Kiencke and Nielsen, 2003).

Engine

The net engine torque (T_e) is the resultant torque from engine combustion ($T_{comb,e}$) after subtracting the torque from engine frictions ($T_{fric,e}$) and the torque used by auxiliary system, such as powersteering and air processor,

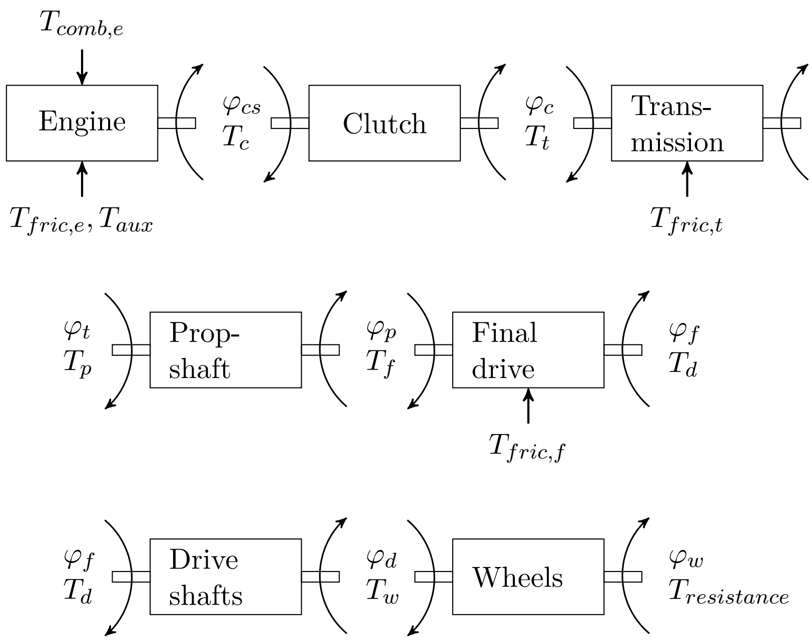

Figure 3.2: Block diagram over the different parts of the driveline that is included in the vehicle model, together with the notations for torques and angles. The figure is based on the figures for the vehicle models presented in (Kiencke and Nielsen, 2003) and (Sahlholm, 2011).

(T_{aux}). The dynamics of the engine is given by Newton's second law

$$J_e\ddot{\varphi}_{cs} = T_{comb,e} - T_{fric,e} - T_{aux} - T_c = T_e - T_c \tag{3.1}$$

where J_e is the engine moment of inertia and φ_{cs} is the angle of the crank shaft.

Clutch

The clutch is used to disengage the crank shaft from the gearbox while shifting gears. The clutch is assumed to be a friction clutch, which is usually found on vehicles equipped with a manual gearbox. Furthermore it is assumed that when the clutch is engaged there is no internal friction, and the model for the clutch thus becomes

$$T_c = T_t \tag{3.2}$$

$$\dot{\varphi}_{cs} = \dot{\varphi}_c \tag{3.3}$$

Transmission

The transmission is one of the parts of the driveline that stands for a significant reduction of the overall driveline efficiency which cannot be neglected.

The friction loss torque in the transmission ($T_{fric,t}$) depends on the input torque to the transmission and on the gear currently in use. For each gear (t) there is a specific gear ratio, denoted i_t, and efficiency, η_t. In (Sahlholm, 2011), the friction loss is described as a percentage of the output torque (T_t). The model for the friction loss in the transmission therefore becomes

$$T_{fric,t} = (1 - \eta_t)\, i_t T_t \tag{3.4}$$

The expression for the transmission can thus be written as

$$T_p = T_t i_t - T_{fric,t} = T_t i_t - (1 - \eta_t)\, i_t T_t = T_t \eta_t i_t \tag{3.5}$$

$$\dot{\varphi}_c = i_t \dot{\varphi}_t \tag{3.6}$$

Propeller shaft

The propeller shaft connects the transmission to the final drive. Since there is no interest in dynamics that occurs during heavy accelerations, the propeller shaft is considered stiff and assumed to be without friction. Hence resulting in

$$T_p = T_f \tag{3.7}$$

$$\varphi_p = \varphi_t \tag{3.8}$$

Final drive

The propeller shaft is connected to the final drive which contains the differential and is used to transfer the torque from the propeller shaft to the drive shafts. The differential consists of a planetary gearbox and in the same way as for the transmission, the gearbox does not have ideal efficiency. Contrary to the transmission, the final drive only has one gear, and thus a fixed gear ratio and gear efficiency. The friction loss for the final drive can in the same way as for the transmission, and according to (Sahlholm, 2011), be written as

$$T_{fric,f} = (1 - \eta_f)\, i_f T_f \tag{3.9}$$

Using the model for the friction loss, the expression for the final drive can be written as

$$T_d = T_f i_f - T_{fric,e} = T_f i_f - (1 - \eta_t)\, i_f T_f = T_f i_f \eta_f \tag{3.10}$$

$$\dot{\varphi}_p = i_f \dot{\varphi}_f \tag{3.11}$$

Drive Shaft

The driven wheels on each side of the vehicle are connected to the final drive via the drive shafts. Since there is only interest in the dynamics when driving in longitudinal direction, it is assumed that the wheels on each side of the vehicle are rotating with the same speed $\dot{\varphi}_w$. Furthermore, as with the propeller shaft, it is assumed that the drive shafts are stiff. This yields

$$T_d = T_w \tag{3.12}$$

$$\varphi_f = \varphi_d \tag{3.13}$$

Wheels

The wheels included in this model are the driven wheels that transforms the torque from the driveline to a force driving the vehicle. If there is no slipping between the driven wheels and the road, the speed of the wheels is given by

$$\varphi_w = \varphi_d \tag{3.14}$$

$$\dot{\varphi}_w = \frac{v}{r_w} \tag{3.15}$$

where r_w is the wheel radius.

As described in (Sahlholm, 2011), when the vehicle is accelerating Newton's second law of motion gives that

$$\ddot{\varphi}_w J_w = T_w - T_{resistance} = T_w - F_{resistance} r_w \tag{3.16}$$

where J_w is the total moment of inertia of all the wheels and $T_{restistance}$ is the torque on the wheels originating from the external forces that acts on the vehicle during driving. These forces is described in depth in section 3.2. Equation (3.16) is used to link the external forces via the driven wheels to the dynamics of the vehicle driveline.

3.2 External Forces

When considering longitudinal dynamics, the external forces acting on a vehicle are according to (Kiencke and Nielsen, 2003) the two resistive forces from the air drag ($F_{airdrag}$) and rolling resistance of the wheels (F_{roll}). The force of gravity due to road grade ($F_{gravity}$), can either be a retarding or accelerating force depending on if the vehicle is travelling uphill or downhill. In figure 3.3 these forces are shown when the vehicle is travelling uphill on a road with road grade α, together with the propulsive force from the vehicles powertrain ($F_{powertrain}$).

3.2.1 Airdrag

The model for the force from the air drag is described in section 2.2.2 and includes information about the wind velocity. The estimators are as earlier described supposed to use sensors commonplace on standard HDVs. Anemometers are not included in the standard sensor range and are as noted difficult

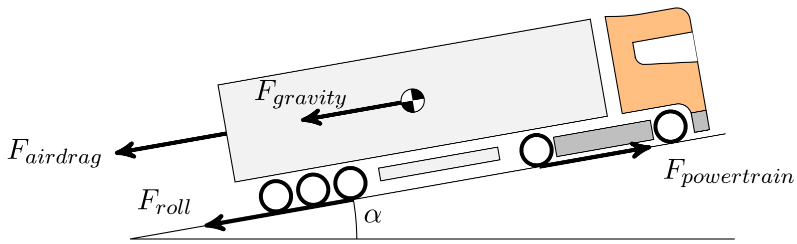

Figure 3.3: The longitudinal forces acting on a vehicle traveling uphill on a road with road grade α.

to install on HDVs without violating legal restrictions. Therefore, the wind speed is not known for the estimators and the model is simplified by assuming that $v_{wind} = 0$. The resulting model becomes

$$F_{airdrag} = \frac{1}{2}\rho_a c_d A_a v^2 \tag{3.17}$$

Almost all modern HDVs are equipped with sensors that measures the temperature and pressure of the ambient air. With this information, the air mass density can be calculated using the ideal gas law, (Ekroth and Granryd, 2006).

Since the calculations of the nominal value of c_d is based on a reference area, only c_d needs to be estimated and not A_a.

3.2.2 Rolling Resistance

The model for the rolling resistance is given in section 2.2.1 as

$$F_{roll} = mg\cos(\alpha)\, c_r \approx mgc_r \tag{3.18}$$

As described in section 2.2.1, several models for c_r has been presented in the literature.

Since the air pressure in the wheels changes with the air temperature according to the ideal gas law, (Ekroth and Granryd, 2006), it is reasonable to use a tire model that includes a temperature dependence. This would however require that the tire temperature would either be measured or estimated during driving in order to perform real-time estimations of the rolling resistance. Some vehicles are equipped with air pressure sensors in the tires and the temperature of the air inside the tires could be approximated using the ideal gas law. However, not all vehicles are equipped with pressure sensors, and in the cases where they are present the accuracy is seldom good enough to determine the actual temperature. Obtaining accurate values of the tire temperature is difficult, and falls outside the scope of this thesis.

Several models for c_r are presented in section 2.2.1 where the rolling resistance includes a speed dependency. If a squared speed term is included, this term would be difficult to separate from the air drag coefficient since both would include the same speed dependency. In the models where a linear speed term is included, the literature has shown that typical values of the linear speed coefficient are considerably lower than both the constant term and squared speed term. It can on the other hand be argued that some driveline losses can be modeled as viscous friction and a linear speed term therefore should be included in the model. Here, they are consider small and are neglected.

The simplest model for the rolling resistance is therefore used in this work, i.e., ignoring velocity and temperature dependence and only considering the force from the rolling resistance as a constant in the vehicle model. Another reason for this choice is the demands on observability, discussed in sections 4.2.1 and 4.3.1.

The sum of the force from the rolling resistance and from the air drag for different vehicle masses and speeds are illustrated in figure 3.4. It can be seen that the force from the rolling resistance for vehicles with large mass is considerably higher than the air drag when travelling at moderate speeds. For the typical case of a vehicle with a mass of 40 [t] travelling at 80 [km/h] on flat road, the air drag corresponds to roughly 40% of the total resistive force while the remaining 60% originates from the rolling resstance.

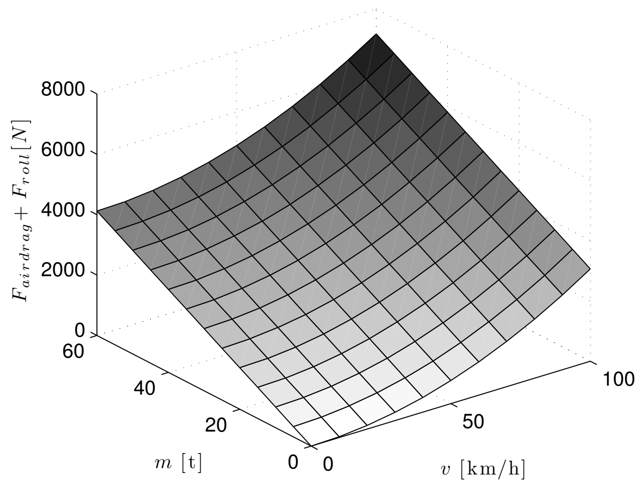

Figure 3.4: Sum of F_{roll} and $F_{airdrag}$ for different vehicle masses and speeds.

3.2.3 Change in Potential Energy

When the vehicle travels on a road with grade α, the force of gravity on the vehicle is according to Newton's second law

$$F_{gravity} = mg \sin \alpha \tag{3.19}$$

As described in section 2.3.2, information about the road grade and vehicle mass is known from map data and from online estimations. This means that $F_{gravity}$ are also known.

3.3 Complete Vehicle Model

By using the equations from section 3.1 and 3.2 the following expression of the vehicle motion can be derived by applying Newton's second law of motion

$$\dot{v} = \frac{1}{m_l} \left(F_{powertrain} - F_{gravity} - F_{roll} - F_{airdrag} \right) \tag{3.20}$$

where $F_{gravity}$, F_{roll} and $F_{airdrag}$ are defined in section 3.2. From the equations in section 3.1 the force $F_{powertrain}$ becomes

$$F_{powertrain} = \frac{i_t i_f n_t n_f}{r_w} T_e \tag{3.21}$$

and the mass m_l becomes

$$m_l = m + \frac{J_w}{{r_w}^2} + \frac{{i_t}^2 {i_f}^2 n_t n_t J_e}{{r_w}^2} \tag{3.22}$$

This vehicle model is identical to the model presented in (Sahlholm, 2011).

3.4 Simulation

The behavior of the vehicle model (3.20) and the effect of incorrect parameter values for c_r and c_d is investigated in this section. The vehicle acceleration is simulated by using data from measurements of a real vehicle in motion as input signals to the vehicle model. A description of the measurements is given in section 5.1.2. By integration of the calculated acceleration signal the simulated vehicle speed is obtained, which in turn is compared to the measured speed of the real vehicle. The vehicle mass was obtained from measuring the weight of the vehicle on a scale.

Six different simulations are performed. In the first three simulations, c_d is set to its nominal value while a different values of c_r is used in each simulation. In the last three simulations, c_r is set to its nominal value while c_d is changed. Table 3.1 shows the different parameter values used in the simulation.

The nominal value of c_d is for vehicles similar to the tractor-semitrailer combination shown in figure 1.2, a large tractor with wind deflectors and a four meters high semitrailer.

Data from two different measurements are used in simulations. Both data sets were collected using the same vehicle driven on the same highway only minutes apart, but on different road segments and during slightly different

Table 3.1: Nominal parameter values and deviations used for the simulation.

Parameter	Nominal value	Deviation
c_r	0.007	$0.007(1 \pm 0.05)$
c_d	0.6	$0.6(1 \pm 0.15)$

wind conditions. In figure 3.5, four sub-figures shows the measured vehicle speed (thick solid line) together with the simulation results for the three different parameter values: below nominal (dotted line), nominal (thin solid line) and above nominal (dashed line). The values used are given in table 3.1. The two upper sub-figures shows the speed for the first road segment, and the lower two shows the speed for the second road segment. In the left sub-figures for each segment has three different values for c_r been used while c_d is set to its nominal value. In the right sub-figures has the nominal value for c_r been used, while the value for c_d is varied.

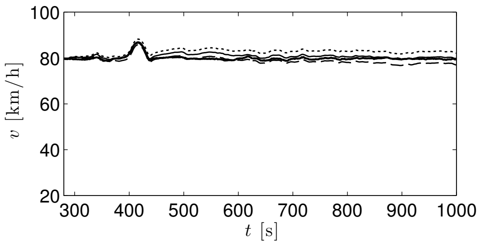

(a) Segment 1. Variations of c_r.

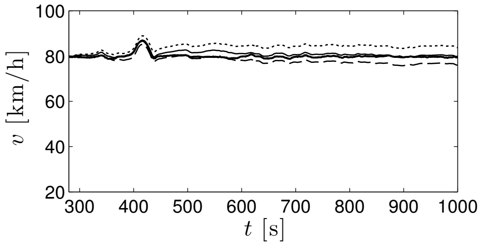

(b) Segment 1. Variations of c_d.

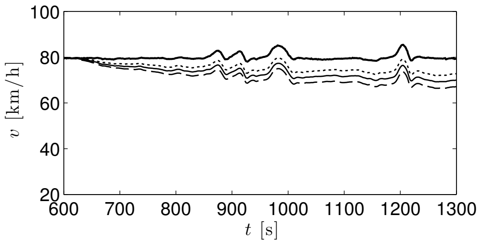

(c) Segment 2. Variations of c_r.

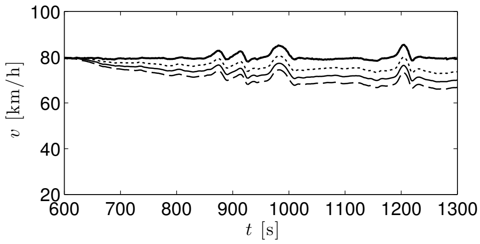

(d) Segment 2. Variations of c_d.

Figure 3.5: Measured speed (thick solid line) and simulated speed when using different values for c_r and c_d, below nominal (dotted line), nominal (thin solid line) and above nominal (dashed line). The two upper sub-figures corresponds to one road segment and the lower two to another. The left and the right sub-figures shows the result for variations in c_r and c_d, respectively.

The figures shows that for the first road segment, the nominal parameter values results in a simulated speed close to the measured speed. Using these values, the simulated speed lies within 5 [km/h] of the measured speed.

For the second road segment, the simulation yields a considerably worse result. Even parameter values below nominal results in a simulated speed well below the measured. A possible cause of the poor match between simulated and measured speed is that the model does not include information on wind speed and direction. Other possible causes is discussed in section 5.2.1. Here it is mainly noted that using this model and input signals, it is to be expected that a large variation in c_r and c_d will be present, even during seemingly similar environmental conditions. The cause might be due to occasional wind gusts or simply that the model is not good enough.

When estimating parameters, a large difference in the systems dynamic response for variations in one of the estimated parameters, compared to the response for variations in another estimated parameter, is beneficial for obtaining accurate estimates. Comparing the two sub-figures for each road segment, it can be seen that for low variations in vehicle speed, the different values of c_r and c_d results in an almost identical dynamic response of the system.

4 Parameter Estimation

In this chapter two different methods for estimating the rolling resistance and the air drag are presented. The first method is the Linear Estimator which is based on a standard Kalman filter and uses a linearized vehicle model. The second method, the Nonlinear Estimator, is based on an extended Kalman filter and uses the nonlinear vehicle model.

The first section describes the process model based on the vehicle model that is used by estimators. The second and third sections details the use of the KF and EKF for the respective estimators, as well as investigates observability and describes estimation algorithms. The last section is dedicated to tune the filters in order to generate accurate estimations.

In case the generated estimations deviate too far from values of c_r and c_d that are physically likely, the estimations are discarded and the nominal values are used. Based on the discussed values of c_d in section 2.2.2 the allowed range for the air drag coefficient is between 0.4 and 0.9. Values outside this region is discarded. For the rolling resistance, the allowed range is between 0.004 and 0.025, based on the discussion in section 2.2.1.

4.1 Augmented Vehicle Model

The parameters c_r and c_d are estimated by augmenting the vehicle model (3.20) with two states corresponding to the parameters. The parameters are assumed to change slow in comparison to the vehicle speed and their derivatives are therefore approximated to zero. The augmentation method is described in (Gustavsson, 2000) and (Höckerdal, 2011) among others. Augmenting the vehicle model thus yields the following process model

$$\underbrace{\begin{bmatrix} \dot{v}(t) \\ \dot{c}_r(t) \\ \dot{c}_d(t) \end{bmatrix}}_{\dot{x}(t)} = \underbrace{\begin{bmatrix} \frac{1}{m_l}\left(F_{powertrain} - F_{grav} - F_{roll} - F_{airdrag}\right) \\ 0 \\ 0 \end{bmatrix}}_{f(x(t),u(t))} + \underbrace{\begin{bmatrix} \omega^{v}(t) \\ \omega^{c_r}(t) \\ \omega^{c_d}(t) \end{bmatrix}}_{\omega(t)} \tag{4.1}$$

The model is discretized using the Euler forward method, described in equation (2.32). With subscript k to indicate discrete time, we get

$$\underbrace{\begin{bmatrix} v_{k+1} \\ c_{r,k+1} \\ c_{d,k+1} \end{bmatrix}}_{x_k} = \underbrace{\begin{bmatrix} v_k + T_s \frac{dv_k}{dt} \\ c_{r,k} \\ c_{d_k} \end{bmatrix}}_{f(x_k,u_k)} + T_s \underbrace{\begin{bmatrix} \omega_k^{v} \\ \omega_k^{c_r} \\ \omega_k^{c_d} \end{bmatrix}}_{\omega_k} \tag{4.2}$$

The process noise is denoted ω_k is the process noise and the process noise covariance becomes $Q_k = E[\omega_k]$.

The sample time T_s is multiplied to the noise ω_k as a direct result of the discretization. Since the actual noise at specific sample intervals is unknown, the column vector ω_k is approximated to zero in the Kalman filter, as described in section 2.4.

4.1.1 Linearized Augmented Vehicle Model

In order to use a standard Kalman filter for parameter estimation, the augmented vehicle model has to be linearized. The equilibrium point of the system is denoted by subscript "eq". The state relative to the equilibrium point is denoted $\tilde{x}$, while $\tilde{u}$ is the input relative to the equilibrium point. Thus $\tilde{x} = x - x_{eq}$ and $\tilde{u} = u - u_{eq}$. The system is linearized by calculating the Jacobian matrix of $f(x(t), u(t))$ in equation (4.1) with respect to the states x and the inputs u, i.e. $J_f(x, u)$. Written on standard state space form the linear system becomes

$$\dot{\tilde{x}}(t) = A\tilde{x}(t) + B\tilde{u}(t) + \omega(t) \tag{4.3}$$

The system matrix A is the columns of the Jacobian matrix corresponding to the partial derivatives with respect to x, i.e., $A = J_f\,(x)\,|_{x_{eq},u_{eq}}$. The control matrix B is the columns from the partial derivatives with respect to u, i.e. $B = J_f\,(u)\,|_{x_{eq},u_{eq}}$. A detailed description of linearization is given in (Glad and Ljung, 2006).

The model will be used for discrete Kalman filtering and it therefore has to be discretized. Using the discretization method in equation (2.31) the state transition matrix F can be approximated by $F = I + AT_s$ and the control matrix by $G = BT_s$, where T_s is the sampling time. This gives

$$\tilde{x}_{k+1} = F\tilde{x}_k + G\tilde{u}_k + \omega_k \tag{4.4}$$

where

$$F = \begin{bmatrix} 1 - T_s\frac{\rho_a A_a}{m_{l,eq}}c_{d,eq}v_{eq} & -T_s\frac{mg}{m_{l,eq}} & -T_s\frac{\rho_a A_a}{2m_{l,eq}}v_{eq}^2 \\ 0 & 1 & 0 \\ 0 & 0 & 1 \end{bmatrix} \tag{4.5}$$

$$G = \begin{bmatrix} T_s\frac{i_t i_f \eta_t \eta_f}{r_w m_{l,eq}} & -T_s\frac{mg}{m_{l,eq}}\cos\alpha_{eq} \\ 0 & 0 \\ 0 & 0 \end{bmatrix} \tag{4.6}$$

Since the dynamics of gear changes are not included in the model, this approach yields a piecewise linear system that is linear between the gear changes. Different linearization points are used for each gear and the matrices F and G thus changes between gears but are otherwise constant.

4.1.2 Measurement Equation

Since the augmented vehicle model is used in a Kalman filter a measurement equation is needed (Sahlholm, 2011). In equation (4.2) the input signals are the net engine torque T_e, the air mass density ρ_a, the vehicle mass m and the road grade α. The only measured signal is the vehicle speed v, and the measurement equation thus becomes

$$y_k = \underbrace{\begin{bmatrix} 1 & 0 & 0 \end{bmatrix}}_{H} \underbrace{\begin{bmatrix} v_k \\ c_{r,k} \\ c_{d,k} \end{bmatrix}}_{x_k} + \underbrace{\begin{bmatrix} e_k^v \end{bmatrix}}_{e_k} \tag{4.7}$$

The measurement noise e_k is assumed to be WGN, and we get the measurement noise variance $R_k = E[e_k^2]$.

4.2 Linear Estimator

In order to investigate the behaviour of the linearized vehicle model, a linear estimator is designed. This section describes how a standard KF can be used for the parameter estimation of the rolling resistance coefficient and the air drag coefficient. Since the standard KF is linear, the linearized augmented vehicle model (4.4) is used. The next section will however show that when the vehicle model is augmented with two states and linearized, it is not observable, and that only one parameter can be estimated.

It is therefore interesting to investigate if the parameters can be estimated one at a time and if these estimations can be based on each other. An estimation algorithm is presented, where the rolling resistance is estimated at low speeds and the air drag at high speeds.

Hence the linearized system is used, all the input and measurement signals to the KF are the variation from the respective equilibrium points, i.e.,

$$\tilde{u}_k = u_k - u_{eq} \tag{4.8}$$

$$\tilde{y}_k = y_k - Hx_{eq} \tag{4.9}$$

The estimated states $\hat{x}$ should therefore be interpreted as the estimated variation from the equilibrium point x_{eq}. When discussing the results from the estimation, x_{eq} will be added to $\hat{x}$ to ease the analysis.

4.2.1 Observability for the Linearized Vehicle Model

In order to ensure that the estimated states from the KF converges towards the true values, the observability of the linearized system (4.3) is investigated. The observability criterion for linear systems is given in equation (2.26).

Calculating the observability matrix for the linearized system system yields

$$\mathcal{O} = \begin{pmatrix} H \\ HA \\ HA^2 \end{pmatrix} \tag{4.10}$$

$$= \begin{pmatrix} 1 & 0 & 0 \\ \frac{1}{m_l} A_a \rho c_{d,eq} v_{eq} & -mg & -\frac{1}{2m_l} A_a \rho c_{d,eq} v_{eq}^2 \\ \frac{1}{m_l^2} \left(A_a \rho c_{d,eq} v_{eq}\right)^2 & -\frac{1}{m_l} A_a \rho c_{d,eq} v_{eq} mg & -\frac{1}{2m_l^2} \left(A_a \rho c_{d,eq} v_{eq}^{3/2}\right)^2 \end{pmatrix} \tag{4.11}$$

where A and H are defined in equations (4.3) and (4.7) respectively.

The rank of this 3×3 matrix is 2. The matrix is hence rank deficient and it can be concluded that the linearized augmented vehicle model is not observable and should therefore not be used for estimation of the coefficients.

This agrees with the results presented in (Höckerdal, 2011), where it is stated that a linear system, on the form of the linearized vehicle model, can only be augmented with as many states as there are measurement signals in order to maintain observability. Since only one signal is measured in this case, the default system can be augmented with only one state.

If the default vehicle model is augmented with one state, corresponding to either c_r or c_d, it can be shown that the augmented system is observable regardless of if c_r or c_d is chosen for estimation. The next section describes an estimator where c_r and c_d are estimated one at a time.

4.2.2 Partial Model Augmentation and Estimation

Since the linearized vehicle model can only augmented to estimate one parameter, this section describes a method for estimating the rolling resistance and air drag one at a time by using the linearized vehicle model and a standard KF. This yields two different modes of the estimator, denoted by subscript m.

Estimating the Air drag

The default nonlinear vehicle model (3.20) is augmented with a second state corresponding to the air drag coefficient c_d and then linearized. The rolling resistance is considered as a known constant and treated as an input signal to the system, since it would otherwise be lost during the linearization.

Choosing the states $x_1 = v, x_2 = c_d$, the nonlinear augmented system becomes

$$\dot{x}_1 = \frac{1}{m_l} \left(\frac{i_t i_f n_t n_f}{r_w} T_e - mg \sin \alpha - mgc_r - \frac{1}{2} A_a \rho_a x_2 x_1^2 \right) + \omega^{x_1} \tag{4.12}$$

$$\dot{x}_2 = \omega^{x_2} \tag{4.13}$$

This expression is linearized and discretized according to the procedure described in section 4.1.1, and writing it on the form of equation (4.4) gives

$$x_k = \begin{pmatrix} v_k \\ c_{d,k} \end{pmatrix}, \qquad u_k = \begin{pmatrix} T_{e,k} \\ \alpha_k \\ c_r \end{pmatrix} \tag{4.14}$$

$$F_m = \begin{pmatrix} 1 - T_s \frac{1}{m_l} A_a \rho_a x_{2,eq} x_{1,eq} & -T_s \frac{1}{2m_l} A_a \rho_a x_{1,eq}^2 \\ 0 & 1 \end{pmatrix} \tag{4.15}$$

$$G_m = \begin{pmatrix} T_s \frac{i_t i_f n_t n_f}{r_w m_l} & -T_s \frac{mg}{m_l} \cos\alpha_{eq} & -T_s \frac{mg}{m_l} \\ 0 & 0 & 0 \end{pmatrix} \tag{4.16}$$

$$H = \begin{pmatrix} 1 & 0 \end{pmatrix} \tag{4.17}$$

The observability criterion in (2.26) is fulfilled for this system, and the system can thus be used for parameter estimation. The condition number defined in equation (2.29) becomes $\kappa = 1.24 \cdot 10^1$ which can be considered fairly well-conditioned.

Estimating the Rolling Resistance

For estimation of the rolling resistance coefficient c_r, the case is similar. The default nonlinear vehicle model (3.20) is augmented with a second state corresponding to c_r. Choosing the states $x_1 = v, x_2 = c_r$, the nonlinear augmented model becomes

$$\dot{x}_1 = \frac{1}{m_l}\left(\frac{i_t i_f n_t n_f}{r_w} T_e - mg\sin\alpha - mgx_2 - \frac{1}{2} A_a \rho_a c_d x_1^2\right) + \omega^{x_1} \tag{4.18}$$

$$\dot{x}_2 = \omega^{x_2} \tag{4.19}$$

Linearizing and discretizing this expression in the same manner as earlier yields

$$x_k = \begin{pmatrix} v_k \\ c_{r,k} \end{pmatrix}, \qquad u_k = \begin{pmatrix} T_{e,k} \\ \alpha \end{pmatrix} \tag{4.20}$$

$$F_m = \begin{pmatrix} 1 - T_s \frac{1}{m_l} A_a \rho_a c_d x_{1,eq} & -T_s \frac{mg}{m_l} \\ 0 & 1 \end{pmatrix} \tag{4.21}$$

$$G_m = \begin{pmatrix} T_s \frac{i_t i_f n_t n_f}{r_w m_l} & -T_s \frac{mg}{m_l} \cos\alpha_{eq} \\ 0 & 0 \end{pmatrix} \tag{4.22}$$

$$H = \begin{pmatrix} 1 & 0 \end{pmatrix} \tag{4.23}$$

Calculating the observability matrix (2.25) it can be shown that the observability matrix has full rank, and the system is hence observable and can be used for estimation. The condition number defined in equation (2.29) becomes $\kappa = 9.71$, which is roughly the same magnitude as κ for the air drag estimator.

4.2.3 Estimation Algorithm

The force from the rolling resistance is as earlier discussed in section 3.2.2, considerably higher than that from the air drag when driving at low speeds. In such cases, a deviation of c_d in equation (3.17) from its true value will only have a small impact on the force from the air drag.

Hence, the rolling resistance is estimated at lower speeds, below 60 [km/h], while the air drag is estimated at higher speeds, above 60 [km/h]. This corresponds to the two different modes for the estimator. During each mode, the parameter that is not being estimated is set to a constant value. If neither the rolling resistance or air drag has been estimated, for example when the vehicle is started, both parameters are set to their nominal values, $c_d = 0.6$, $c_r = 0.007$. Once a parameter has been estimated, the estimated value is used during the estimation of the other parameter.

The algorithm can be summarized as

1. If $v < 60$ [km/h] estimate c_r.
   - If $\hat{c}_d$ exists, use $c_d = \hat{c}_d$
   - Otherwise use $c_d = 0.6$.
2. If $v > 60$ [km/h] estimate c_d.
   - If $\hat{c}_r$ exists, use $c_r = \hat{c}_r$
   - Otherwise use $c_r = 0.007$.

Consider the typical scenario where a vehicle is driven at low speeds towards a highway. During this phase the rolling resistance is estimated and the nominal value of c_d is used. When the vehicle reaches the highway and the speed is increased, the estimation of the rolling resistance is stopped and the the air drag is estimated, based on the estimated value of the rolling resistance.

However, as described in section 2.2.1, the rolling resistance is dependent on the tire temperature. In section 5.2.1 this dependency is shown through experiments. Estimations of the air drag should therefore not be performed based on estimations of the rolling resistance made with cool tires. By monitoring the vehicle speed and the time, estimations of the rolling resistance can be made after the vehicle has been driven at high speed for at least one hour and the stationary tire temperature thus has been reached.

Events not covered by the model, such as gear shifts and braking, are handled as detailed in section 4.4.3. If any of the parameters converges to a value outside the allowed region, the estimation is restarted with the corresponding nominal value.

4.3 Nonlinear Estimator

This section describes the use of an EKF for the parameter estimation. Since the EKF is a nonlinear filter it used the nonlinear augmented vehicle model (4.2).

4.3.1 Observability for the Nonlinear System

The observability matrix for nonlinear systems is given in equation (2.27) as

$$\mathcal{O} = \begin{pmatrix} dh \\ dL_f h \\ \vdots \\ dL_f^{n-1} h \end{pmatrix} \tag{4.24}$$

Calculating the observability matrix for the nonlinear augmented vehicle model (4.1) results in quite cumbersome expressions and are not given explicitly here. By performing the calculations and applying the observability criterion (2.28) it can however be shown that the system is observable as long as the vehicle speed is nonzero.

To further investigate the feasibility to use an EKF, the detectability of the linearized system (4.3) is calculated. The definition of detectability is given in section 2.4.2. The observability matrix for the linearized system is calculated in section 4.2.1, see equation (4.11). There, it is shown that the matrix only has two linearly independent equations. However, it can also be seen that the none of the modes are both unstable and unobservable. Therefore, the necessary detectability criterion is fulfilled and an EKF can be applied.

4.3.2 Algorithm

The nonlinear estimator generate estimations of both coefficients simultaneously and continuously as long as the vehicle speed is higher than 60 [km/h]. Demands on input signals and events such as gear shifts and breaking are managed through adaption of the process noise covariance matrix, as detailed in section 4.4.3. If any of the estimated parameters converges to a value outside the allowed region, these values are discarded. The estimation is then restarted and initiated with the nominal values.

4.4 Filter Tuning

Two of the main challenges that comes with this type of parameter estimations are that, firstly, the physically correct covariance matrix Q and variance R are not known. Instead they becomes tuning parameters in order to tune the filters to generate accurate estimations. Secondly, in order to tune the filter, the the true values of c_r and c_d must be known. This is generally not the case.

The process noise covariance Q is chosen as a diagonal matrix in order to reduce the number of tuning parameters. Together with the measurement noise variance R this gives four tuning parameters: the process noise variance for $\hat{v}$, $\hat{c}_r$, $\hat{c}_d$ and the measurement noise variance for v. As earlier described in section 2.4.1, the initial value of P also effects the filter performance.

The filter tuning is performed in two steps. In the first step, the vehicle model is used to simulate the input and measurement signal. In the second step, a coast down test is performed, similar to the ones described in 2.3.1. The steps are described in sections 4.4.1 and 4.4.2, respectively. The purpose of the two steps is to tune Q and R in order to generate accurate estimations.

4.4.1 Simulation method

The basic concept of the simulation method for the filter tuning is shown in figure 4.1.

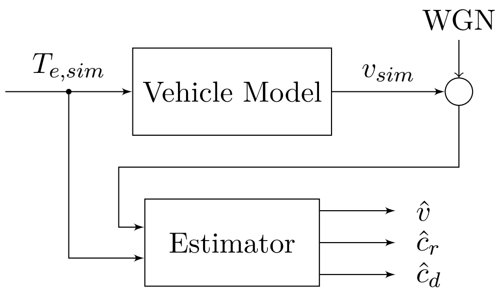

Figure 4.1: The vehicle model is used to generate a torque signal $T_{e,sim}$ and a speed signal v_{sim}. By using these as input signals to the estimator, the filters can be tuned in order generate accurate estimations.

From the vehicle model (3.20), the engine torque signal is calculated based on the nominal values for c_r and c_d. The torque signal is then given as input to the vehicle model and the vehicle speed is calculated. In other words, it is assumed that the vehicle model is a perfect description of the true system by creating input signals based on the model itself. The true values of c_r and c_d are therefore known.

When driving at constant speed, the engine torque based on the model becomes

$$T_{e,sim} = \frac{r_w}{i_t i_f n_t n_f}\left(mg\sin(\alpha) - mgc_r - \frac{1}{2}\rho_a A_a c_d v^2\right) \tag{4.25}$$

where the nominal values for c_r and c_d is used. For the simulation are two different torque signals created, based on equation (4.25), $T_{e,sim}^{sin}$ and $T_{e,sim}^{step}$, where

$$T_{e,sim}^{sine} = \begin{cases} T_{e,sim} + \sin(\omega t) & \text{if } t = \left[2\frac{4\pi}{\omega}, 4\frac{4\pi}{\omega}\right], \omega = \frac{1}{4\pi} \\ T_{e,sim} & \text{otherwise} \end{cases} \tag{4.26}$$

$$T_{e,sim}^{step} = \begin{cases} 0 & \text{if } t = [125, 150] \\ T_{e,sim} & \text{otherwise} \end{cases} \tag{4.27}$$

To the simulated speed signal, WGN is added and is together with the generated torque signal given as measurement and input signals to the estimators, respectively. Since the true values for the parameters to be estimated are known, Q and R can be tuned in order to obtain as accurate estimates as possible.

The estimation result for torque signals $T_{e,sim}^{sine}$ and $T_{e,sim}^{step}$ when used with the linear estimator are shown in figure 4.2.

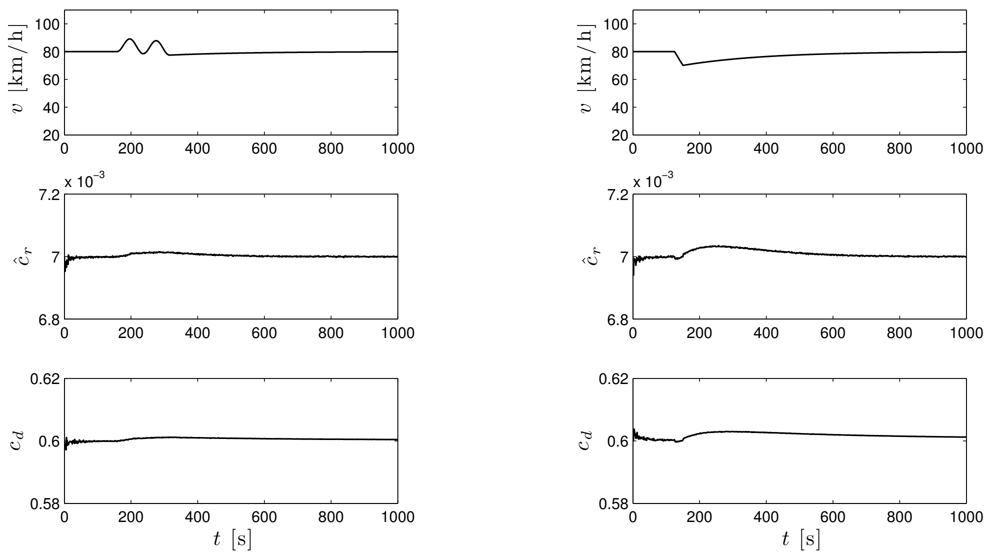

(a) Input signal $T_{e,sim}^{sine}$.

(b) Input signal $T_{e,sim}^{step}$.

Figure 4.2: Simulation results for the linear estimator. The estimations of $\hat{c}_r$ and $\hat{c}_d$ are done one at a time, based on the nominal value of the parameter that is not estimated.

The first part of the figures shows the vehicle speed while the second and third part shows the estimated states, $\hat{c}_r$ and $\hat{c}_d$. The corresponding elements of the estimated error covariance matrix P_k are not shown in the figure. Here it is only stated that $P_{(2,2)}$ quickly converges to a low value, close to $5 \cdot 10^{-6}$ if c_r is estimated and $3 \cdot 10^{-2}$ if c_d is estimated, regardless of input signal. As described in section 4.2, the linear estimator only estimates one parameter at a time, during which the nominal value for the other parameter is used. During these simulation, the two parameters have been estimated using the same input and measurement signals.

The result when using the nonlinear estimator with the two torque signals is shown in figure 4.3 where also the diagonal elements of P_k corresponding to $\hat{c}_r$ and $\hat{c}_d$ is included.

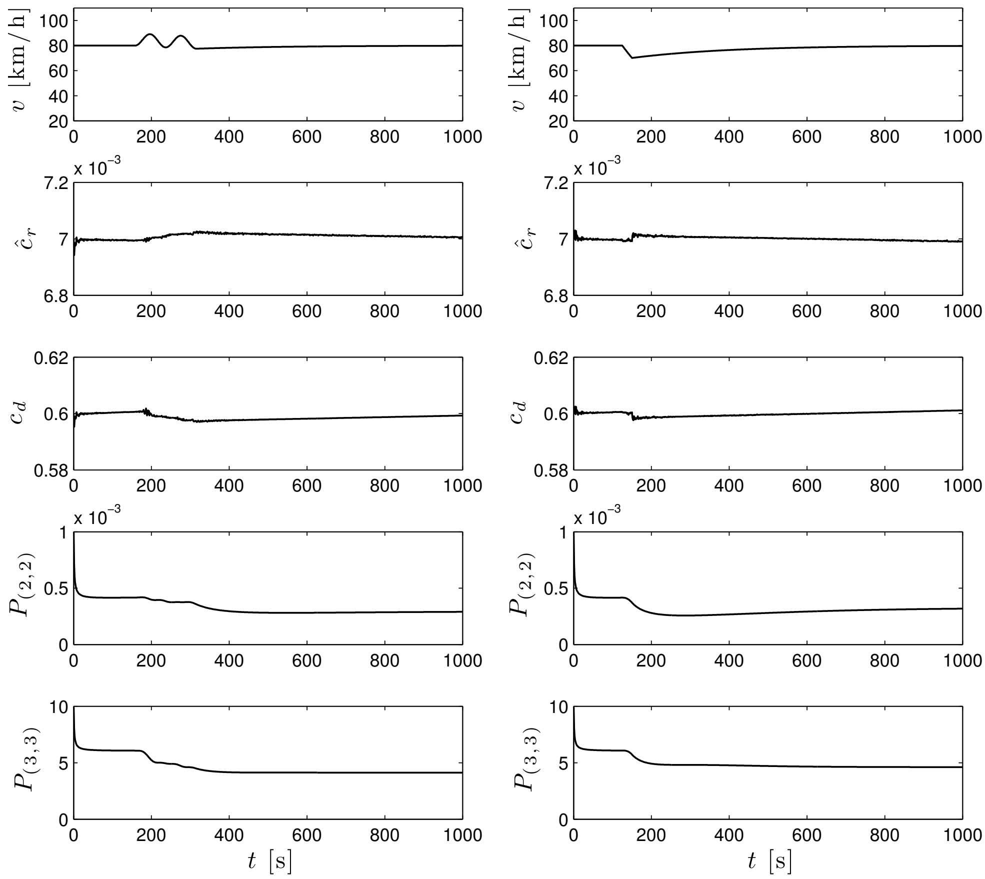

(a) Input signal $T_{e,sim}^{sine}$.

(b) Input signal $T_{e,sim}^{step}$.

Figure 4.3: Results from noninear estimator used with input signal $T_{e,sim}^{sine}$, sub-figure (a), and $T_{e,sim}^{step}$, sub-figure (b).

Both the linear and nonlinear estimator are able to generate accurate estimates for the two torque inputs.

When the speed variation is introduced, a reaction in the estimated states can be noted. For the nonlinear estimator, a reduction in the magnitude of the estimated error variance for both parameters can be noted when the speed variation occurs, indicating that the estimator becomes more certain of the estimations.

A difference when comparing the linear and the nonlinear estimator can be found when studying the curve profile of the estimated states. In the nonlinear case, after the speed variation is introduced, $\hat{c}_r$ displays a linear decrease while $\hat{c}_d$ shows a linear increase. The estimated values are still close to the true values, but the figures clearly indicate how $\hat{c}_r$ and $\hat{c}_d$ complement each other – looking almost like each others mirror images.

The results from the simulations are given in table 4.1, together with the RMSE value for each estimated parameter. As seen in the table, all estimations are accurate and the RMSE value is low.

Table 4.1: Kf and EKF estimates of c_r and c_d and corresponding RLSE value, based on simulated signals

Parameter	Torque type	Estimated value	RMSE
$\hat{c}_r^{KF}$	sine	0.007001	$6.9968 \cdot 10^{-3}$
$\hat{c}_d^{KF}$	sine	0.6004	$5.9945 \cdot 10^{-1}$
$\hat{c}_r^{KF}$	step	0.006999	$6.9908 \cdot 10^{-3}$
$\hat{c}_d^{KF}$	step	0.6012	$5.9819 \cdot 10^{-1}$
$\hat{c}_r^{EKF}$	sine	0.007006	$1.3381 \cdot 10^{-5}$
$\hat{c}_d^{EKF}$	sine	0.5993	$1.6201 \cdot 10^{-3}$
$\hat{c}_r^{EKF}$	step	0.006991	$6.3160 \cdot 10^{-6}$
$\hat{c}_d^{EKF}$	step	0.6011	$7.6795 \cdot 10^{-4}$

As mentioned above, when using the KF to estimate the rolling resistance, the estimated error covariance $P_{(2,2)}$ quickly converges to a considerably low value, close to $5 \cdot 10^{-6}$. The effect of low values on P_k is discussed in section 2.4.1. Although it is preferable that the estimated value is close to the true value, a low value of P_k can have drawbacks. If the value of the true state for some reason would change, a low value of P_k could cause the filter to react slower to that change than desired. In fact, the convergence could be so low that it would in practice barely be noticeable.

Several practical issues can cause such behaviour of the true value of the rolling resistance, for example if the road surface changes from asphalt to gravel, the road temperature suddenly changes due to variations in weather condition etc. To account for such events, a lower limit is set to $P_{(2,2)}$. The limit is chosen to $1 \cdot 10^{-5}$ and when this value is reach, $P_{(2,2)}$ is increased to $1 \cdot 10^{-4}$. The effect is shown in figure 4.4. At time $t = 100$ [s] c_r is increased

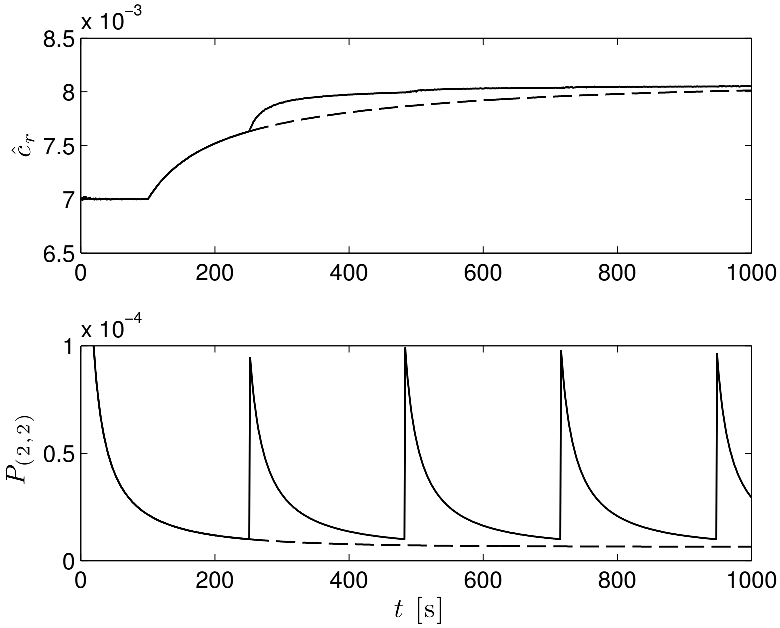

Figure 4.4: Estimated rolling resistance and corresponding element of P. The solid line shows the result when a lower limit is set for $P_{(2,2)}$ and the dashed line shows the results when any value of $P_{(2,2)}$ is allowed.

from its nominal value 0.007 to 0.008. A constant simulated torque signal is used causing the vehicle speed to decrease when c_r is increased. The first part of the figure shows $\hat{c}_r$. The dashed line shows the result when the $P_{(2,2)}$ is allowed to converge at any value, while the solid line shows the result when the boundary value is used. The second part shows a close up on $P_{(2,2)}$ for both cases. From the figure it can be seen that as soon $P_{(2,2)}$ reaches the limit and is increased, the estimated state quickly response. The limit is chosen to obtain as fast convergence as possible while keeping the ripple in $\hat{c}_r$ as low as possible. If the limit of $P_{(2,2)}$ is set to $1 \cdot 10^{-5}$ and is not increased once reaching the limit, the estimated state converges slowly. If the limit instead is set to $1 \cdot 10^{-4}$ the noise originating from the measurement signal is less suppressed.

Although $P_{(2,2)}$ converges to a low value, it is still high enough for the filter to respond to changes without the limit.

4.4.2 Coast Down Test

In order to further tune the filters, a coast down test was performed similar to the ones described in section 2.3.1. A test vehicle was driven on flat road towards a downhill segment with a constant speed of 60 [km/h]. Upon entering the downhill segment, the driveline was disengaged and the vehicle was allowed to freely coast downhill. This caused the vehicle to accelerate due to the its mass and the negative road grade. When the topography of the road changed and an uphill segment was reached, the speed reduced until it reached 60 [km/h] and the test was ended. During the test, signals was measured and stored as detailed in section 5.1.2.

Based on the measured signals, an offline least-squares estimation (LSE) of c_r and c_d is performed. For details about LSE, see for example (Kailath et al., 2000). Writing the vehicle model (3.20) on standard LSE format yields

$$\left[\frac{i_t i_f n_t n_f}{r_w} T_e - \dot{v} m_l - mg \sin\alpha\right] = \left[\frac{1}{2}\rho_a A_a v^2, mg\right] \begin{bmatrix} \hat{c}_d^{LSE} \\ \hat{c}_r^{LSE} \end{bmatrix} \tag{4.28}$$

The acceleration signal is determined by differentiating the measured speed of the vehicle. Since the LSE does not include any tuning steps, the resulting parameter values can be seen as the "true" values. Of course, the result is still be affected by wind and other environmental conditions, but can be regarded as good indicators when tuning the KF and EKF. The results from the LSE are shown in table 4.2.

Based on the results from the simulations in the last section, Q and R are further tuned in order to obtain accurate estimations compared to the results from the LSE. Due to the large speed variation during the coast down test, only the nonlinear estimator is used for the parameter estimation. For the linear estimator, the speed variation is too large for the linearization to be valid.

Using the nonlinear estimator with the further tuned Q and R on the same data set as the LSE yields the results shown in figure 4.5. The first part of the figure shows the measured speed. The second part shows the road grade. The third and fourth parts of the figure shows the estimated states $\hat{c}_r$ and $\hat{c}_d$, while the two last parts shows the corresponding estimated error variances $P_{(2,2)}$ and $P_{(3,3)}$. The estimation starts at $t = 180$ [s], and from the figure it can be seen that both estimated states converges once system is subject to a high excitation. When the vehicle is coasting at constant speed before the downhill segment, only a small reduction in the magnitude of $P_{(3,3)}$ can be noted. It is not until the vehicle is travelling downhill and a large speed variation is introduced that the magnitude of $P_{(3,3)}$ is considerably reduced. Studying the plots of the estimated states also shows that it is the large speed variation that causes the states to converge.

Ideally, the vehicle should have been let to continue to coast until it reached a lower speed, preferably around 20 [km/h]. Since the mass of a HDV is large, it needs to cover a long distance in order to reduce the speed when traveling on roads with moderate grades. Additionally, the test was performed on an open road with traffic. Finding a situation ideal for coast down tests is difficult, and the figure shows the best case obtained.

The estimated parameter values from the nonlinear estimator are given in table 4.2, together with the RMSE value for each parameter when assuming

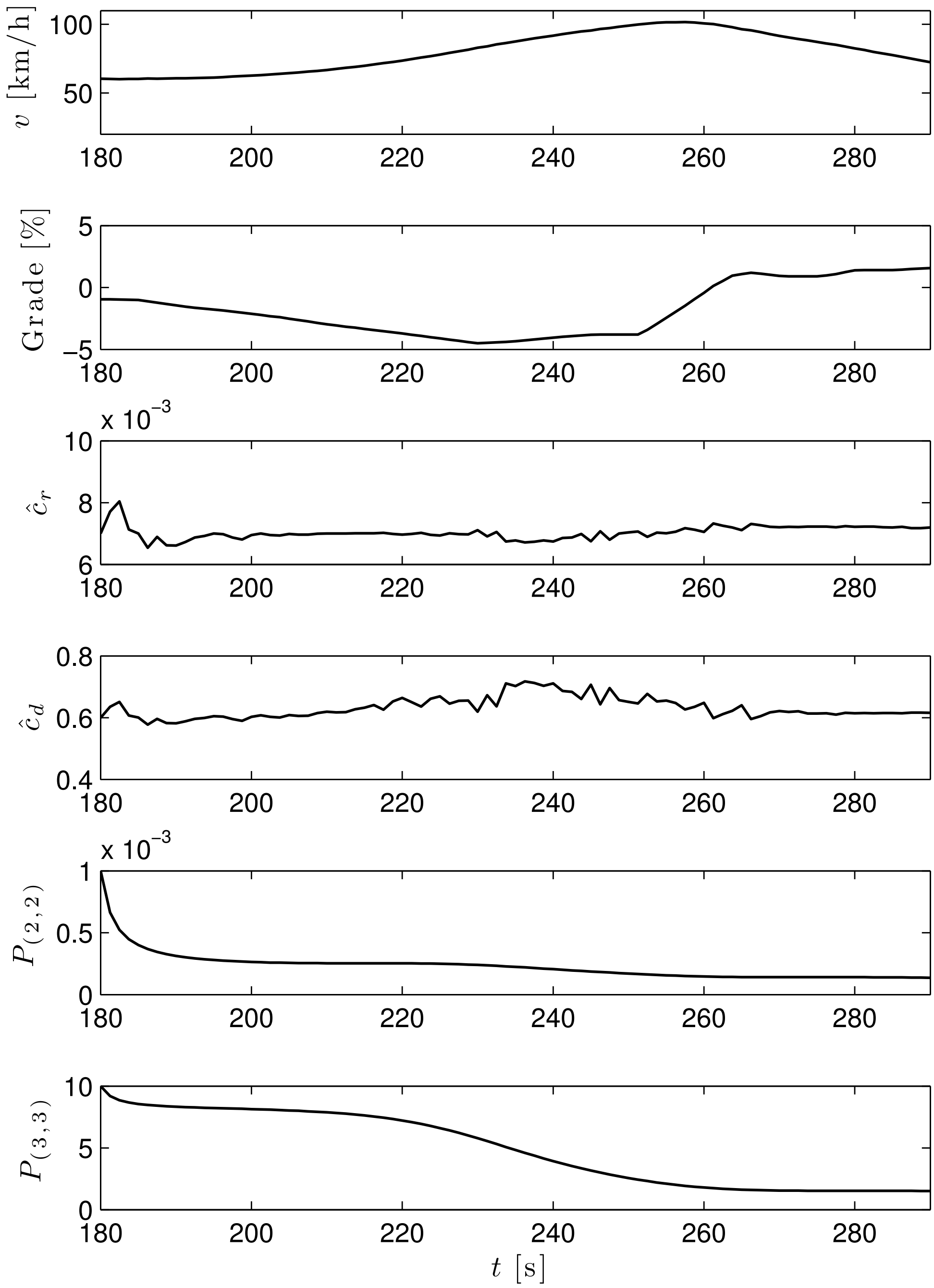

Figure 4.5: EKF estimation results from coast down test. The measured speed is shown together with the estimated parameters and corresponding elements of the estimated error covariance matrix.

that the LSE generated the true values. It can be seen that after tuning, the estimator was able to generate accurate results when comparing to the LSE estimation.

Table 4.2: EKF and LSE estimates of c_r and c_d and corresponding RMSE values.

Parameter	Estimated value	RMSE
$\hat{c}_r^{LSE}$	0.007182	0.007353
$\hat{c}_r^{EKF}$	0.007192	
$\hat{c}_d^{LSE}$	0.6167	0.7351
$\hat{c}_d^{EKF}$	0.6154	

4.4.3 Selection of Q, R and P

Based on the simulation method and on training data from typical driving scenarios, the following process noise covariance, measurement noise variance and initial value for the estimated error covariance is selected.

For the linear estimator when estimating c_r, the Q_k, R_k and $P_{k,0}$ are chosen as

$$
\begin{aligned}
Q_k^{KF,c_r} &= \begin{pmatrix} 1 \cdot 10^2 & 0 \\ 0 & 1 \cdot 10^{-4} \end{pmatrix} \\
R_k^{KF,c_r} &= 1 \cdot 10^{-4} \\
P_{k,0}^{KF,c_r} &= \begin{pmatrix} 1 \cdot 10^1 & 0 \\ 0 & 1 \cdot 10^{-1} \end{pmatrix}
\end{aligned}
$$

When estimating c_d, the following selections were made

$$
\begin{aligned}
Q_k^{KF,c_d} &= \begin{pmatrix} 1 \cdot 10^2 & 0 \\ 0 & 1 \cdot 10^{-5} \end{pmatrix} \\
R_k^{KF,c_d} &= 1 \cdot 10^{-4} \\
P_{k,0}^{KF,c_d} &= \begin{pmatrix} 1 \cdot 10^1 & 0 \\ 0 & 1 \cdot 10^{-1} \end{pmatrix}
\end{aligned}
$$

For the nonlinear estimator, the following values was selected based on the simulation method, the coast-down test and on training data from typical driving scenarios

$$Q_k^{EKF} = \begin{pmatrix} 1 \cdot 10^2 & 0 & 0 \\ 0 & 1 \cdot 10^{-6} & 0 \\ 0 & 0 & 1 \cdot 10^{-5} \end{pmatrix}$$
$$R_k^{EKF} = 1 \cdot 10^{-4}$$
$$P_{k,0}^{EKF} = \begin{pmatrix} 1 \cdot 10^{-2} & 0 & 0 \\ 0 & 1 \cdot 10^{-3} & 0 \\ 0 & 0 & 1 \cdot 10^{1} \end{pmatrix}$$

Since neither the dynamics of gear shifts or braking is included in the vehicle model, estimations should not be performed during these events. To account for this, the same method as described in (Sahlholm, 2011) is used. The process noise variance for the speed state is increased, in this case to $1 \cdot 10^{10}$, causing the filter to act with a large uncertainty on the vehicle model with the effect that the estimations of c_r and c_d are hold. It is assumed that sharp turns, also not covered by the model, occurs together with gear shifts, breaking or when driving at low speeds, below 30 [km/h]. Therefore, no estimations are performed when driving below 30 [km/h]. Analysis the steering wheel angle or vehicle yaw rate is left out in order to minimize the signal dependency.

5 Experiments

This chapter describes the experiments that has been conducted in order to collect training data and investigate the performance of the estimators. The first section describes the experimental setup and details the equipment used and signals measured. The second section describes the results from using the estimation methods on logged data.

5.1 Experimental Setup

Three different test vehicles was used during a total of three experiments. The experiments were conducted by driving the test vehicles on public roads and measuring important signals. These are described in section 5.1.2.

The experiments were conducted on the same roads, but under different environmental conditions. Some in conditions with both high wind gusts and windless situations, as well as on both dry and wet asphalt.

Since road testing is quite time consuming, none of the different vehicle configurations was driven on the same day as another. Consequently, the environmental conditions were not the same during the different experiments. The estimation results will hence depend on both the test vehicle but also on the environmental conditions at the time of the experiment.

In order to investigate how large excitation of the system is required to generate accurate estimations, the vehicles were driven in three different modes. The purpose is to obtain data from different variations in vehicle speed and to be able to detect if the estimations are sensitive to the behaviour of the engine torque signal. A step-like mode was used where the speed was kept constant for two minutes, and then changed with 10 [km/h]. The vehicles were driven at the new speed for another two minutes where upon the speed was changed again. Another mode was used where the acceleration pedal was used to generate an engine torque signal that resembles of a square wave with different frequencies and amplitudes. This caused the vehicle speed to smoothly vary with 1 to 10 [km/h]. Additionally the vehicles were driven at 80 [km/h] for longer time periods, typically around 20 minutes, in order to obtain data from more normal driving scenarios.

5.1.1 Test Vehicles

Since the important parameters of a HDV can display a large variation between different vehicle configurations, three different test vehicle configurations was used during the experiments. These are shown in figure 5.1 and a general description for each vehicle is given in table 5.1.

It is not difficult to imagine that the air drag coefficient for the three test vehicles are different. Since the value of the coefficient is as earlier described based on the same standard area for all the test vehicles, a smaller value of the estimated c_d is expected for vehicle C, since its true area is smaller. The coefficient of the rolling resistance is on the other hand more difficult to anticipate. As described in section 2.2.1 has earlier work indicated that c_r is not dependent on the number of wheel axles.

Figure 5.1: The three vehicle configurations that was used in the experiments. A tractor-semitrailer combination (test vehicle A), a box-body truck (test vehicle B) and a smaller distribution truck (test vehicle C). Images courtesy of Scania CV AB.

Table 5.1: General information on the test vehicles used for the experiments.

Vehicle	Type	Configuration	Mass [t]
A	R480 LA 4x2 MNA	Tractor-semitrailer	37.5
B	R480 LB 6x2*4 MLB	Truck	21.5
C	P280 LB 4x2 MNB	Distribution truck	12.5

5.1.2 Measured Signals

All the signals that are used by the estimators are broadcast on the vehicles CAN-bus. During the experiments these signals were logged using a PC laptop connected to the network via a CAN interface card. This allowed for offline estimations during the development and evaluation of the estimators.

The input signals to the estimators are as described in section 4.1.2, the net engine torque T_e, the ambient air temperature and pressure that are used to calculate the air mass density ρ_a, the vehicle mass m and road grade α. The current gear is also broadcast and used together with look-up tables to determine the gear ratio i_t and gear efficiency η_t. The gear ratio and efficiency for the final drive, i_f and η_f, are also available on the network. The broadcast vehicle mass is based on estimations with an accuracy often reasonable close to the correct value. The mass used in the experiments are obtained from measuring the weight using a scale. The net engine torque is given as a percentage of the maximum torque for that particular vehicle. The measured vehicle speed originates from the angular velocity of the front axle, which is accurate assuming that the are no slipping between tires and road.

As described in section 4.4.3, other signals are used to determine the process noise covariance matrix of the estimators. Since the vehicle model does not include dynamics when brakes are used, the brake pedal position is monitored. Estimating the actual force from the brake is difficult and extending the model with brake dynamics is left for future work. The model does not include gear changes either, and a signal reporting when gear shifts occurs is therefore monitored.

Furthermore, the estimations of c_r and c_d are as earlier described dependent on weather conditions, such as rain and wind. The Swedish Transport Administration has several weather stations placed alongside roads in Sweden in a project called the Road Weather Information. Data from these weather stations are available from the Swedish Transport Administration homepage[1]. These data are updated every thirty minutes and gives information about air and road temperature as well as mean and maximum wind speed and wind direction. This information has been useful when evaluating the estimators.

5.2 Experimental Results

The performance of the estimators are evaluated by analyzing the results from the road tests. The first section investigates the linear estimator and the nonlinear estimator is investigated in the second section.

5.2.1 Linear Estimator

As described in section 4.2, the linear estimator uses a standard KF and estimates only one parameter at a time. The rolling resistance at lower speeds and the air drag at higher. The performance is evaluated by using data from a typical driving scenario where the driver starts driving on small roads at lower speeds for a short period of time and thereafter driven on top gear on a highway at 80 [km/h] for a longer period of time, to finally turn of the highway and drive on smaller roads again.

Test vehicles B and C was used for the experiments studied in this section. The experiment were divided into the three following steps,

- Step 1. Immediately after start, the vehicles were driven on a straight country road at 50 [km/h]. The tire temperature was therefore equal to the ambient air temperature when the tests were started, close to 10°

[1] `http://trafikinfo.trafikverket.se/litmenu/litmenu.htm#id=380`. Accessed March 1, 2012

Celsius. During the discussion this is referred to as driving with cool tires. The vehicles were driven at both directions on the same road. The first direction had a negative road grade and this road segment is therefore denoted the *downhill road segment*, the opposite direction is naturally denoted the *uphill road segment*. The vehicles were driven at each direction for close to 2 minutes.

- Step 2. The vehicles were driven on a highway at 60 to 85 [km/h] for one hour, allowing the temperature in the tires to reach stationary value. Here, the different driving modes described in section 5.1 was used.

- Step 3. Immediately after the vehicles were driven off the highway, they were once again driven on the uphill and downhill road segments on the country road at 50 [km/h], but now with a tire temperature corresponding to highway driving. This is referred to as driving with warm tires.

Figures 5.2 and 5.3 shows the interesting signals when driving with cool tires on both the downhill and the uphill road segment. The first figure shows the signals for test vehicle B and the second figure for test vehicle C. As the two experiments were not conducted on the same day but the environmental conditions, such as road and wind conditions and temperature, were similar.

The first part of the figures shows the measured vehicle speed while the second part shows the engine torque, as a percentage of the maximum torque available from the engine. The third part shows the road grade. Since the vehicles were driven on the same road the road grade signals are identical, but the engine torque signals differs mainly due to the difference in mass and engine power. The fourth part of the figure shows the current gear (solid line) and whether the vehicle is braking or not (dashed line). The estimated rolling resistance $\hat{c}_r$ is shown in the last part of the figure. The effect from braking and shifting are highly noticeable, as the estimation is paused during those events, as well as when driving below 30 [km/h].

A close up on the estimated rolling resistance for the two vehicles is given in figure 5.4. From these figures an interesting observation can be made. It can be seen that $\hat{c}_r$ quickly converges to seemingly reasonable values. However, it can also be noted that $\hat{c}_r$ converges to a higher value when driving on the downhill road segment compared to when driving on the uphill road segment. Test vehicle B uses different gears when driving in the two directions while test vehicle C uses the same gear in both direction. Despite this, the same behavior of $\hat{c}_r$ is noted for both experiments.

The source of this uncertainty can likely be found in the engine torque signal. Since the vehicles are traveling slightly downhill in the first segment and slightly uphill in the second, the force $F_{gravity}$ is negative in the first segment and positive in the second. This results in a difference in the engine torque required to keep steady speed between the two segments.

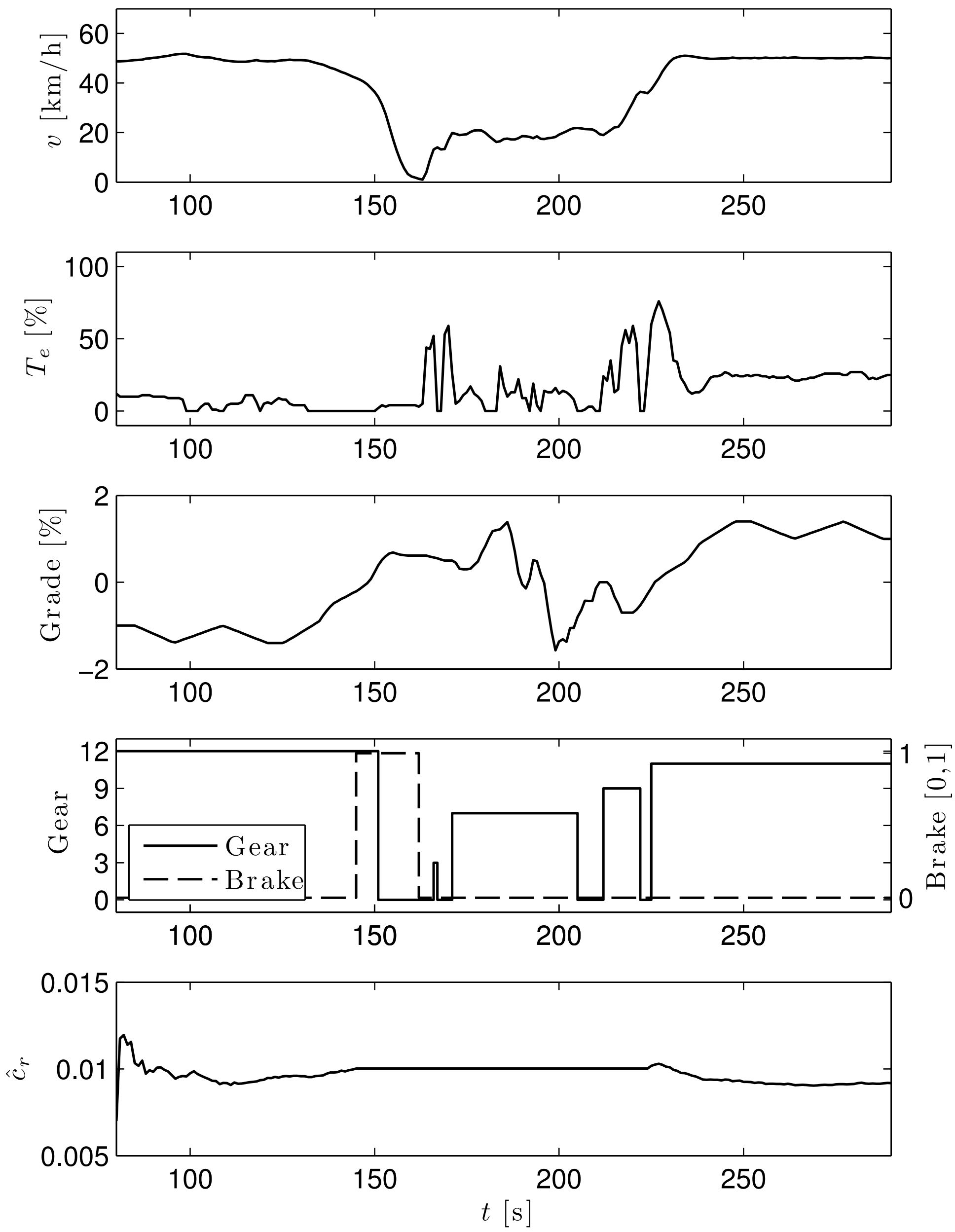

Figure 5.2: Signals of interest for test vehicle B when driving with cool tires on the downhill road segment ($t = [50\ 100]$ [s]) and the uphill road segment ($t = [175\ 225]$) [s]. The vehicle is turned around in a roundabout during $t = [100\ 175]$ [s]. Estimation generated by the linear estimator. $P_{(2,2)}$ converges towards $1.8 \cdot 10^{-7}$.

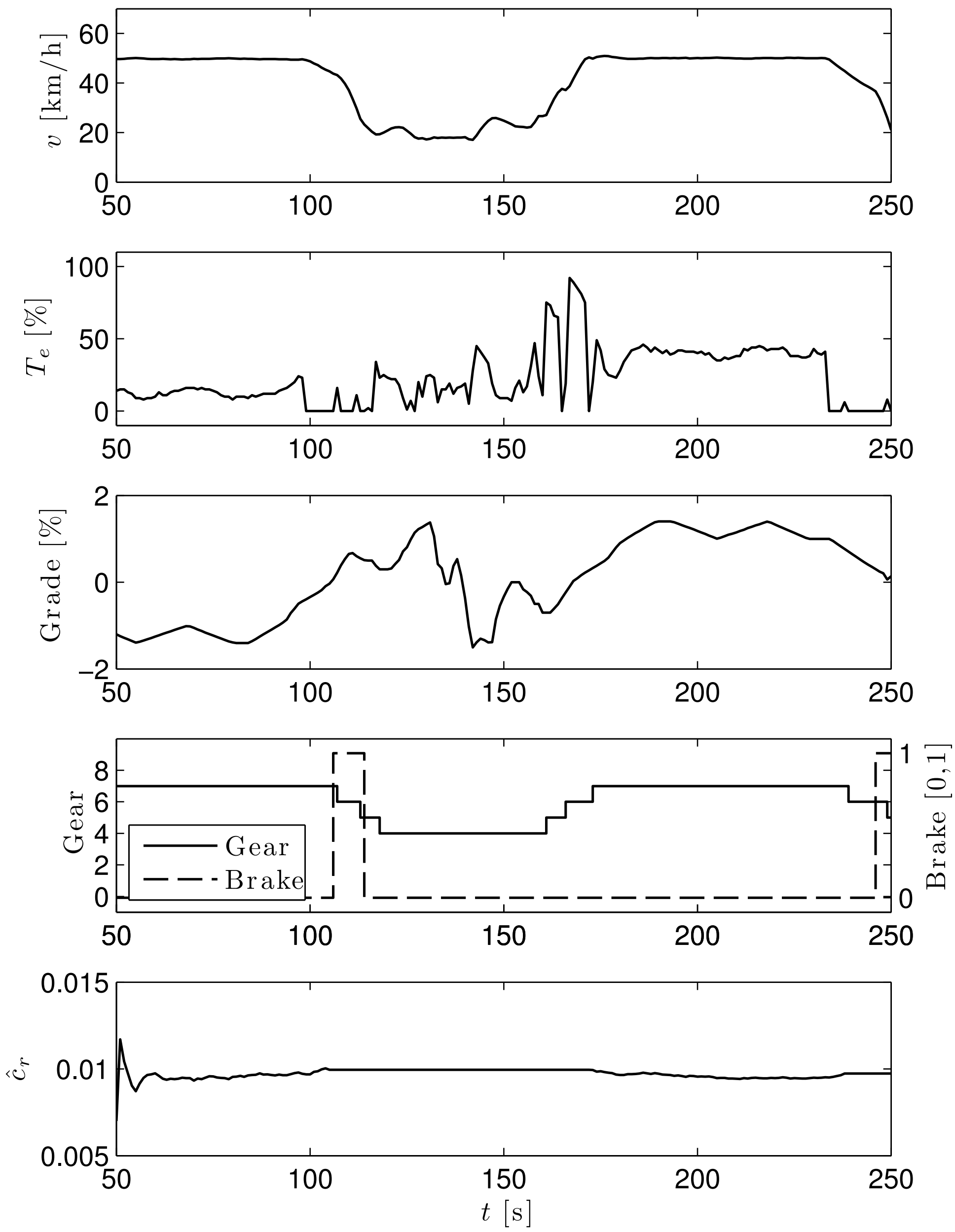

Figure 5.3: Signals of interest for test vehicle C when driving with cool tires on the downhill road segment ($t = [75\ 150]$ [s]) and the uphill road segment ($t = [225\ 275]$ [s]. The vehicle is turned around in a roundabout during $t = [150\ 225]$ [s]. Estimation generated by the linear estimator. $P_{(2,2)}$ converges towards $2.0 \cdot 10^{-7}$.

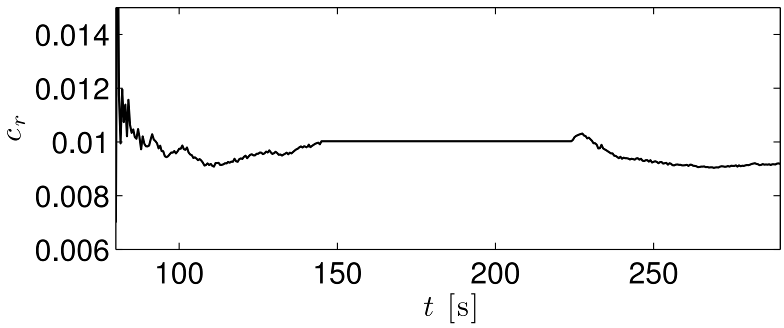

(a) Test vehicle B.

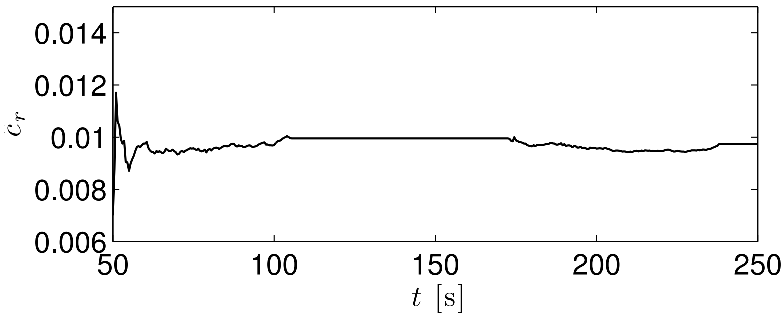

(b) Test vehicle C.

Figure 5.4: A closer look at $\hat{c}_r$ for test vehicles B and C from figures 5.2 and 5.3 respectively. The estimations are generated by the linear estimator while the vehicles are driven on the downhill and uphill road segment with cool tires.

The engine torque signal is based on an estimation and does not describe the actual torque with perfect accuracy. Furthermore, it is given as a percentage of the maximum torque, and consequently decreases the resolution of the estimation with higher values of the maximum torque. Since the maximum torque of the engine is known, the torque signal is most reliable when the engine is producing maximal torque. It is therefore not impossible that the estimated rolling resistance from the uphill road segment is the most accurate of the two.

The results from the estimations with both cold and warm tires for the two vehicles are given in table 5.2. The warm tires corresponds to the tire temperature after the one hour highway drive. The table shows the estimated values for both the downhill and uphill road segment.

As seen in the table, it is only when test vehicle C is driven with warm tires that the estimations generated on the downhill road segment are lower than for the uphill road segment. A possible cause of this behaviour might be a high wind speed during the experiment.

Table 5.2: Estimation results of c_r generated by the linear estimator.

Test vehicle	Tire condition	$\hat{c}_r$ (downhill segment)	$\hat{c}_r$ (uphill segment)
B	cold	0.0100	0.0092
B	warm	0.0057	0.0055
C	cold	0.0100	0.0097
C	warm	0.0068	0.0082

Comparing the estimated rolling resistance with cold and warm tires, it can be seen that a higher tire temperature yields a lower value of $\hat{c}_r$. This corresponds well with the results in (Sandberg, 2001) and (Wong, 2001) as discussed in section 3.2.2.

Because of this temperature dependency, it can be concluded that the problem stated for the estimation algorithm in section 4.2.3 is reasonable. It is difficult to estimate c_d based on earlier estimates of c_r, generated at a time when the tire temperature was different from the tire temperature at which the estimation of c_d is performed.

Another conclusion can be drawn from the values in table 5.2. The estimated value of c_r is almost identical for the two test vehicles when driven with cool tires, despite the difference in number of wheel axles. This agrees with the earlier presented work in section 2.2.1. When driving with warm tires the estimated value is however different for the two vehicles. Once again, the cause might be wind speeds for the experiment with test vehicle C with warm tires.

Figure 5.5 shows the interesting signals for test vehicles B and C, when driving on the highway segment and estimating the air drag c_d. No gearshifts or braking occurs during the presented road segments. The first part of the figure shows the measured speed (solid line) and the simulated speed (dashed line). The second part shows the net engine torque while the estimations of c_d is shown in the last. The simulated speed is based on the estimated value of c_d. These estimations are based on the nominal value for c_r.

As seen in the figures, $\hat{c}_d$ converges to reasonable values for both test vehicles. As discussed in section 3.4, the nominal value of $c_d = 0.6$ is valid for the larger test vehicles A and B, while a lower value of c_d is expected for test vehicle C since the its actual area is smaller than the standardized area. By comparing the two figures, it can be noted that both the speed and the engine torque signal for test vehicle B displays a larger variation in magnitude compared to the signals for test vehicle C. The speed for the latter is close to constant and the engine torque is kept around 50 %. Regardless of this variation between the two experiments, the estimator is able to generate accurate results. The variation in the engine torque for vehicle B causes however the estimation of c_d to converge slower. For both cases converges $P_{(2,2)}$ quickly towards $1 \cdot 10^{-4}$.

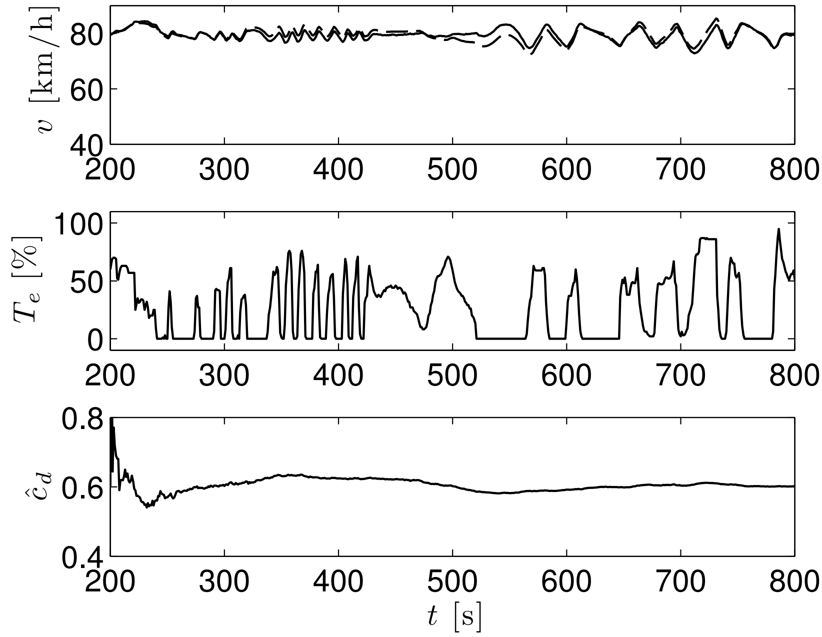

(a) Test vehicle B. At $t = 750$ s has $\hat{c}_d$ converged to 0.60.

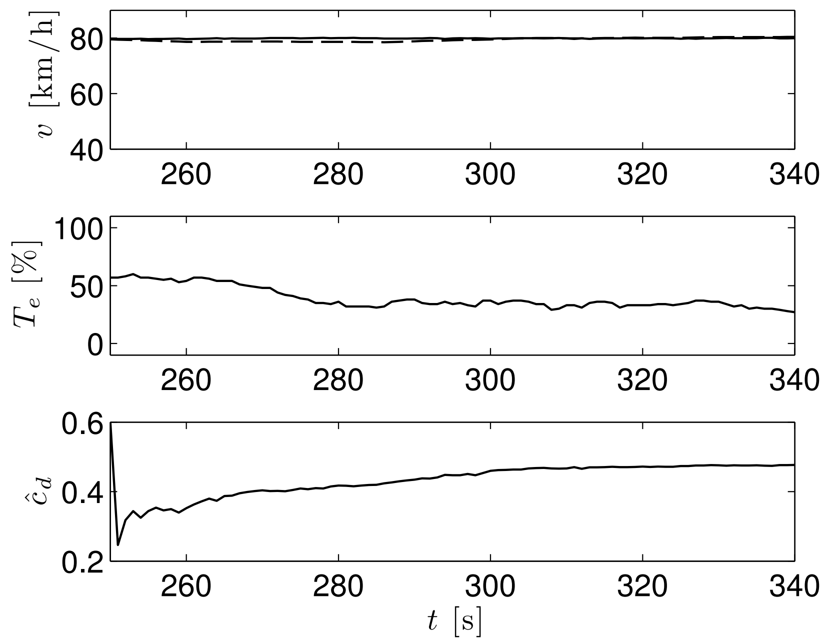

(b) Test vehicle C. At $t = 310$ s has $\hat{c}_d$ converged to 0.48.

Figure 5.5: Signals of interest when using the linear estimator on test vehicle B (sub-figure a) and C (sub-figure b) when estimating c_d.

5.2.2 Nonlinear Estimator

The nonlinear estimator is investigated using the same experimental data as the linear estimator in the previous section. Additionally, test vehicle A is used. The experiments with this test vehicle is not used for the linear estimator, since the vehicle was not driven on the downhill and uphill road segment.

Two different scenarios of the estimations are shown in figures 5.6 for test vehicle C and 5.7 for test vehicle A. The first part of the figures shows the measured and simulated speed. The engine torque is shown in the second part. Part three and four shows the estimated rolling resistance and air drag, while the corresponding elements of the estimated error covariance matrix are shown in the last two parts of the figure. The simulation of the vehicle speed shown in the first part of the figure is performed offline and is based on the values of the estimated states at the last time step shown in the figures.

As seen from the first figure, both the vehicle speed and engine torque are close to constant. Although the estimated states converges to reasonable values, the magnitude of $P_{(2,2)}$ is barely reduced when compared with the simulations in section 4.4.1.

The second figure shows the opposite case. The vehicle speed is close to 80 [km/h] for the majority of the presented road segment, apart from at time $t = 200$ [s] and $t = 400$ [s] where the speed is increased with 5 [km/h] for 40 seconds and 10 [km/h] for 80 seconds, respectively. In this figure it can be seen that the estimated states show no sign of convergence, but rather a divergence. The estimated rolling resistance decreases over time as the estimated air drag increases. Neither one of the estimated states show any sign of reaching a boundary value. The magnitude of $P_{(2,2)}$ and $P_{(3,3)}$ is on the other hand reduced from the initial values and behaves similar to the simulations in section 4.4.1. It can be noted that the magnitude is further decreased during the larger speed variation. Although the estimated states does not converge, the corresponding modes of the system are most likely observable since neither $P_{(2,2)}$ or $P_{(3,3)}$ increases linearly. By studying $P_{(2,2)}$ for vehicle A and B it can be seen that the the magnitude is reduced considerably for vehicle A compared to vehicle B.

However, the difference between the simulated speed and the measured speed is in both figures relatively small, especially when comparing to the vehicle model simulation in section 3.4. This indicates that the sum of the forces from the estimated rolling resistance and air drag are accurate, although they are not individually correct.

During the coast down test described in section 4.4.2, the nonlinear estimator was able to generate accurate results for both c_r and c_d while the magnitude of $P_{(2,2)}$ and $P_{(3,3)}$ was considerably reduced from the initial values. Compared to the more common driving scenarios presented in this section, the two major differences are in the vehicle speed and the engine torque signals. The speed variation during the coast down test is considerably higher than those presented here. The torque signal in figure 5.6 is without larger variations, while the torque signal in figure 5.7 is uneven and reaches all values between 0 to 100 %. During the coast down test the transmission was in neutral and no engine torque was transferred through the powertrain.

From this it can be concluded that in order to generate accurate estimations, a speed variation higher than that found during normal driving situations is required.

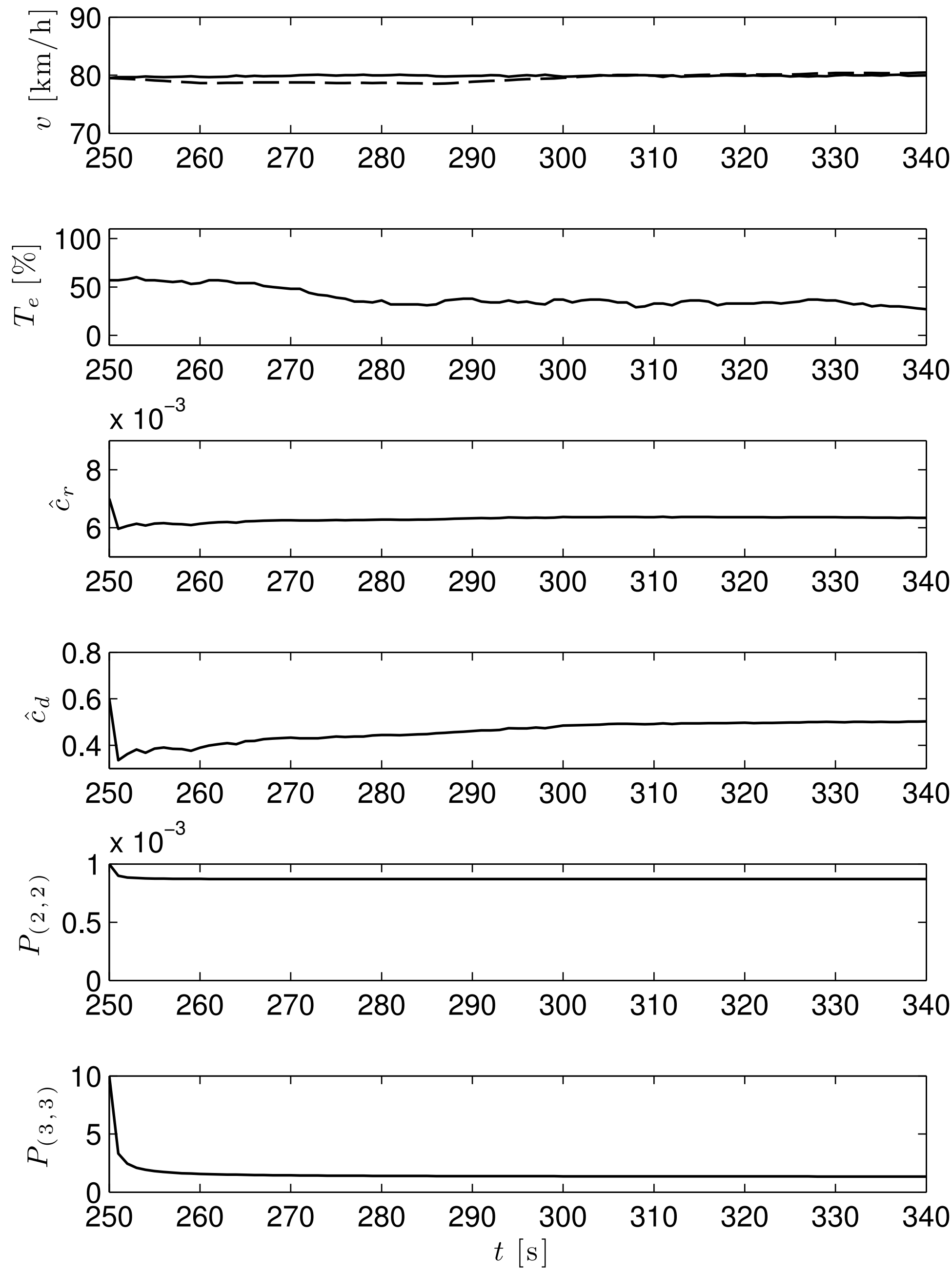

Figure 5.6: Signals of interest for the fist road segment with test vehicle C. The estimated states shows a convergence at $t = 300$ [s]. However, only a small reduction of the magnitude of P can be noted.

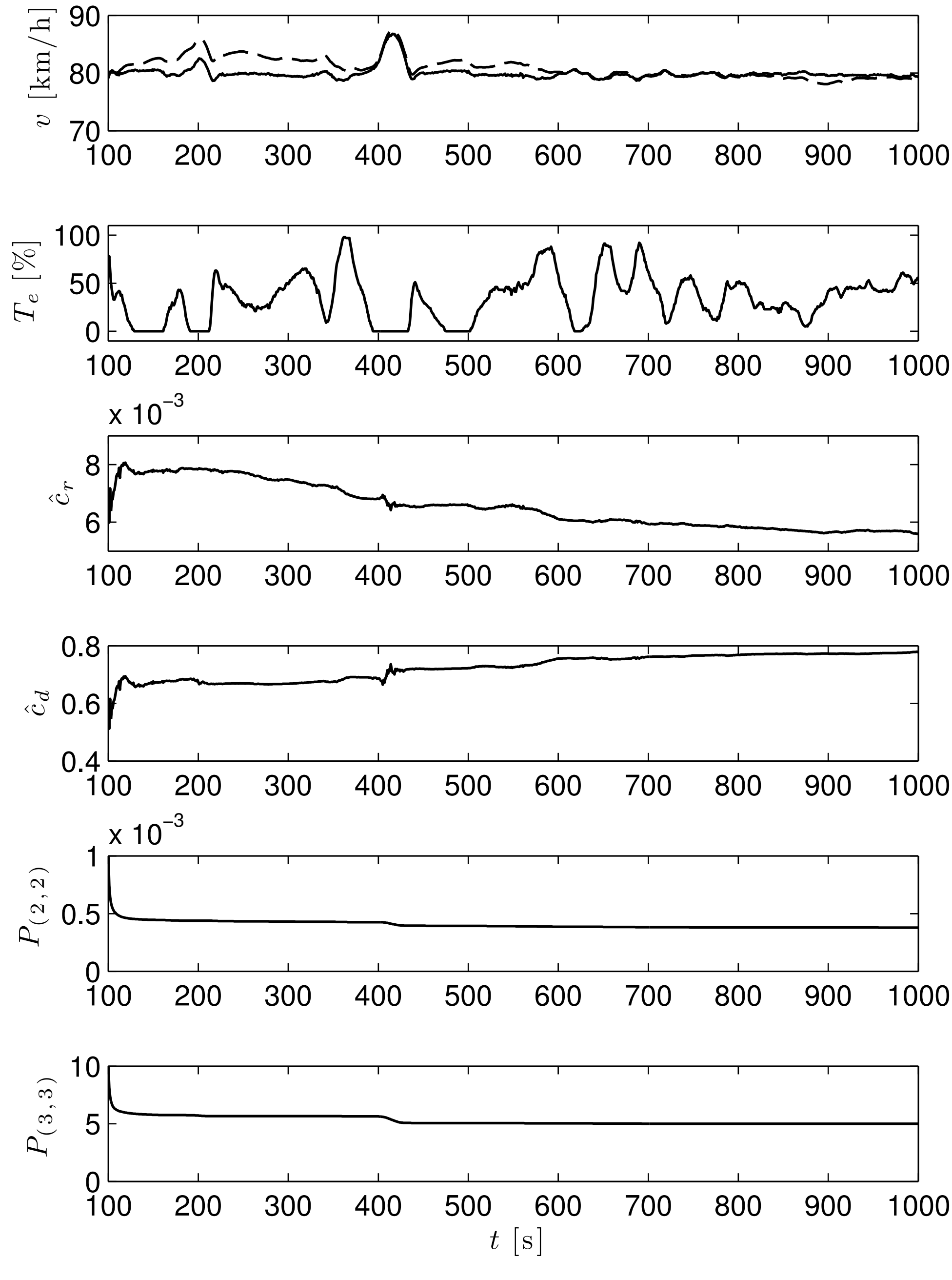

Figure 5.7: Signals of interest for the fist road segment with test vehicle A. The estimated states $\hat{c}_r$ and $\hat{c}_d$ show no sign of convergence to values close to the nominal values.

6 Conclusions and Future Work

This chapter presents the conclusions that can be drawn based on the simulations and experiments of the proposed estimations methods and describes areas for future work.

6.1 Conclusions

A vehicle model has been developed in Chapter 3 which is used by the suggested estimators to generate estimation of the rolling resistance and the air drag. Simulations have shown that accurate values of the estimated parameters are of great importance to obtain a valid model. The presented model is commonly used in the field of automotive control and accurate parameter values are important to achieve good vehicle control.

As described in Chapter 4, two different Kalman filters have been used for the estimations, one being the standard Kalman filter which uses a linearized vehicle model. The other is an extended Kalman filter which uses the default nonlinear model. It has been shown that due to demands on observability, the linearized model can not be used to estimate both parameters at the same time. Therefore, an estimator based on a standard Kalman filter is proposed, which estimates one parameter at a time, basing the estimates on each other.

From the experimental results in Chapter 5 it has been shown that when estimating one parameter accurate results can be obtained. However it is also shown that the temperature dependency of the rolling resistance makes it difficult to base estimations on each other in practice. The estimations of the air drag should only be based on an earlier estimate of the rolling resistance if both the following conditions are true: The estimated rolling resistance is generated at a low speed, during a time when the tire temperature is equal or close to the corresponding stationary temperature when driving at high speed. A real case would be to perform the estimation of the rolling resistance shortly after the vehicle has left a highway after being driven there for one hour or more.

Additionally, the number of wheel axles has not shown any influence on the total force from the rolling resistance in the conducted experiments. This corresponds well with the presented previous work, as does the temperature dependency of the rolling resistance.

Further in Chapter 5, it has been shown that the extended Kalman filter is able to generate accurate estimations. However, due to the complementary nature of the parameters discovered during the simulations, the extended Kalman filter is only able to do so if a large speed variation is present. For the presented coast down test the estimates show accurate convergence, while no convergence was found for more common driving scenarios. In practice, it is difficult to find speed variations that are large enough, since the model is not valid during hard accelerations and braking.

The purpose of the project is as stated in section 1.2 to suggest methods for online estimation of the air drag and rolling resistance. With the above, the purpose has been partly fulfilled since the suggested methods, mainly the nonlinear estimator, works during the discussed conditions. In practice however, it has been shown that it is difficult to find situations ideal for the estimations. The main thesis contribution has been to describe possible usage of the standard and the extended Kalman filter to solve the problem.

6.2 Future Work

Other nonlinear filters than the extended Kalman filter used in this thesis, such as a particle filter, may be more suitable for the estimation problem. In this work, the possibilities to use different Kalman filters was investigated. They are commonly used and are relatively easy to implement and requires reasonable system resources. Investigation of other methods, for example the particle filter, is proposed for future work.

Variations in rolling resistance and air drag are two error sources for functions controlling the vehicle. However, the wind speed, that has been neglected in this work, most likely stands for a significant error source as well. Estimations of the wind speed and direction are therefore suggested for future work.

Bibliography

H. S. Bae and J. C. Gerdes. Parameter estimation and command modification for longitudinal control of heavy vehicles, 2003. California Partners for Advanced Transits and Highways (PATH).

I. Ekroth and E. Granryd. *Tillämpad termodynamik*. Studentlitteratur AB, 1:st edition, 2006.

T. Glad and L. Ljung. *Control Theory: Multivariable and Nonlinear Methods*. Taylor & Francis Ltd, 1 edition, 2000.

T. Glad and L. Ljung. *Reglerteknik: grundläggande teori*. Studentlitteratur AB, 4:th edition, 2006.

F. Gustavsson. *Adaptive Filtering and Change Detection*. John Wiley & sons, Ltd, 2000.

W. Hucho et al. *Aerodynamics of Road Vehicles*. SAE International, 4:th edition, 1998.

E. Höckerdal. *Model Error Compensation in ODE and DAE Estimators with Automotive Engine Applications*. Doctoral thesis, Linköping University, Linköping, Sweden, 2011.

ISO 11898-1:2003. *Road vehicles – Controller area network (CAN) – Part 1: Data link layer and physical signalling*. ISO, 2003.

T. Kailath et al. *Linear Estimation*. Prentice Hall, 2000.

U. Kiencke and L. Nielsen. *Automotive Control Systems*. Springer Verlag, 2003.

P. Misra and P. Enge. *Gobal Positioning Systems: Signals Measurement and Performance*. Ganga Jamuna Press Lincon Mass, 2:nd edition, 2006.

C. C. Paige. Properties of numerical algorithms related to computing controllability. *IEEE Transactions of Automatic Control*, AC-26(1), februari 1981.

P. Sahlholm. *Distributed Road Grade Estimation for Heavy Duty Vehicles*. Doctoral thesis, Royal Institute of Technology (KTH), Stockholm, Sweden, 2011.

T. Sandberg. *Heavy Truck Modeling for Fuel Consumption. Simulations and Measurements*. Licentiate thesis, Linköping University, Linköping, Sweden, 2001.

A. Vahidi, A. Stefanopoulou, and H. Peng. Recursive least squares with forgetting for online estimation of vehicle mass and road grade: Theory and experiments. *Journal of Vehicle System Dynamics*, 43:31–35, januari 2005.

W. Walston, F. Buckley, and M. Colin. Test procedures for the evaluation of aerodynamic drag on full-scale vehicle in windy environments. *SAE Technical Paper 760106*, 1976.

R. White and H. Korst. The determination of vehicle drag contributions from coast-down tests. *SAE Technical Paper 720099*, 1972.

Y. Y. Wong. *Theory of Ground Vehicles*. John Wiley & Sons, 3:rd edition, 2001.